Article

Chemical Characterization and Source Apportionment of PM$_{10}$ Using Receptor Models over the Himalayan Region of India

Nikki Choudhary [1,2], Akansha Rai [1,2], Jagdish Chandra Kuniyal [3], Priyanka Srivastava [4], Renu Lata [5], Monami Dutta [6], Abhinandan Ghosh [7], Supriya Dey [8], Sayantan Sarkar [8], Sakshi Gupta [1,2], Sheetal Chaudhary [3], Isha Thakur [5], Archana Bawari [3], Manish Naja [4], Narayanasamy Vijayan [1,2], Abhijit Chatterjee [6], Tuhin Kumar Mandal [1,2], Sudhir Kumar Sharma [1,2,*] and Ravindra Kumar Kotnala [1,2]

1   CSIR-National Physical Laboratory, Dr. K. S. Krishnan Road, New Delhi 110012, India;
    nikkichoudhary1607@gmail.com (N.C.); akansharai.may@gmail.com (A.R.);
    sakshigupta21096@gmail.com (S.G.); nvijayan@nplindia.org (N.V.); tuhinkumarmandal@gmail.com (T.K.M.);
    rkkotnala@gmail.com (R.K.K.)
2   Academy of Scientific and Innovative Research (AcSIR), Ghaziabad 201002, India
3   G. B. Pant National Institute of Himalayan Environment, Kosi-Katarmal, Almora 263643, India;
    jckuniyal@gmail.com (J.C.K.); sheetalchaudharyshitu@gmail.com (S.C.); archanabawari123@gmail.com (A.B.)
4   Aryabhatta Research Institute of Observational Sciences (ARIES), Nainital 263002, India;
    psrivastava@aries.res.in (P.S.); manish@aries.res.in (M.N.)
5   G. B. Pant National Institute of Himalayan Environment, Himachal Regional Centre,
    Mohal-Kullu 175126, India; renu15_negi@yahoo.co.in (R.L.); isha950414@gmail.com (I.T.)
6   Environmental Sciences Section, Bose Institute, EN Block, Sector-V, Saltlake, Kolkata 700091, India;
    monamidutta2509@gmail.com (M.D.); abhijit.boseinst@gmail.com (A.C.)
7   Department of Civil Engineering, Centre of Environmental Science and Engineering, IIT-Kanpur,
    Kanpur 201086, India; abhinandan1011@gmail.com
8   School of Civil and Environmental Engineering, Indian Institute of Technology Mandi, Kamand 175005, India;
    supriyadey08@gmail.com (S.D.); sayantan@iitmandi.ac.in (S.S.)
*   Correspondence: sudhir@nplindia.org or sudhircsir@gmail.com

Abstract: This study presents the source apportionment of coarse-mode particulate matter (PM$_{10}$) extracted by 3 receptor models (PCA/APCS, UNMIX, and PMF) at semi-urban sites of the Indian Himalayan region (IHR) during August 2018–December 2019. In this study, water-soluble inorganic ionic species (WSIIS), water-soluble organic carbon (WSOC), carbon fractions (organic carbon (OC) and elemental carbon (EC)), and trace elements of PM$_{10}$ were analyzed over the IHR. Nainital (62 ± 39 μg m^{-3}) had the highest annual average mass concentration of PM$_{10}$ (average $\pm$ standard deviation at $1\,\sigma$), followed by Mohal Kullu (58 ± 32 μg m^{-3}) and Darjeeling (54 ± 18 μg m^{-3}). The annual total $\sum$WSIIS concentration order was as follows: Darjeeling (14.02 ± 10.01 μg m^{-3}) > Mohal-Kullu (13.75 ± 10.21 μg m^{-3}) > Nainital (10.20 ± 6.30 μg m^{-3}), contributing to 15–30% of the PM$_{10}$ mass. The dominant secondary ions (NH$_4^+$, SO$_4^{2-}$, and NO$_3^-$) suggest that the study sites were strongly influenced by anthropogenic sources from regional and long-range transport. Principal component analysis (PCA) with an absolute principal component score (APCS), UNMIX, and Positive Matrix Factorization (PMF) were used for source identification of PM$_{10}$ at the study sites of the IHR. All three models showed relatively similar results of source profiles for all study sites except their source number and percentage contribution. Overall, soil dust (SD), secondary aerosols (SAs), combustion (biomass burning (BB) + fossil fuel combustion (FFC): BB+FFC), and vehicular emissions (VEs) are the major sources of PM$_{10}$ identified by these models at all study sites. Air mass backward trajectories illustrated that PM$_{10}$, mainly attributed to dust-related aerosols, was transported from the Thar Desert, Indo-Gangetic Plain (IGP), and northwestern region of India (i.e., Punjab and Haryana) and Afghanistan to the IHR. Transported agricultural or residual burning plumes from the IGP and nearby areas significantly contribute to the concentration of carbonaceous aerosols (CAs) at study sites.

Keywords: secondary aerosols; water-soluble ionic species; aerosol acidity; neutralization factor; PMF; Himalaya

1. Introduction

The impacts of aerosols on the environment, climate, and human health have been the subject of extensive research in recent decades [1,2]. By reflecting and absorbing the sun's radiation, aerosol particles disrupt Earth's radiation balancing, affecting cloud and rainfall formation by acting as cloud condensation nuclei and ice nuclei [3–6]. Aerosols influence trace atmospheric gases through chemical changes and multiphase processes [7–9]. Aerosol particles can be of primary or secondary origin: primary when released directly from the source and secondary when gas-phase transformations or atmosphere modifications of primary particle components occur.

Carbonaceous aerosols (CAs) compose the majority of particulate matter (PM) in the atmosphere and affect atmospheric chemistry and visibility [1,10–14]. CA combustion and emissions produce hazardous gases, organics, and hydrocarbons that harm the respiratory and cardiovascular systems [15–18]. To comprehend the reactions of primary aerosols in the atmosphere via a gas-to-particle conversion process, water-soluble inorganic ionic species (WSII$_S$) are crucial. Gases such as SO_2 and NO_2 emitted from sources are oxidized and converted to sulfate (SO_4^{2-}) and nitrate (NO_3^-) particles through various heterogeneous reaction pathways. The reactions of secondary species produce ammonium sulfate ((NH_4)$_2SO_4$), ammonium bisulfate (NH_4HSO_4), and ammonium nitrate (NH_4NO_3) [19–21]. The trace and heavy elements in PM_{10} have become particularly known for their toxicity, carcinogenicity, and widespread distribution in recent years [22]. Anthropogenic (Ni, Cr, Zn, Cd, Ni, and Cu) and soil/crustal/road dust tracers (Al, K, Fe, Mg, Ca, Na, Si, and Ti) are two of the most prevalent categories of elemental emissions found in PM [23]. Trace and heavy elements emissions are exacerbated by non-exhaustive factors such as brake and tire wear (Mn, Fe, Zn, Cu, Ba, Cr, Si, and Pb) and exhaust emissions (Zn, Pb, Cr, V, Mn, Fe, Ca, Co, As, Ni, Cd, and Mo) [24–27]. Various health-related issues are linked to trace metals, such as memory loss, respiratory problems, irritation of the nose and throat, dermatitis, and lung cancer [28–32].

Numerous research studies have demonstrated that the composition of PM is pivotal for assessing its impacts on air quality, climate, and human health [33–40]. The atmospheric particles are highly dynamic in concentration and chemical characterization over space and time frames. Any transformation in aerosols' composition can profoundly affect their hygroscopicity, cloud condensation nuclei (CCN), biological activities, chemical reactivity, and optical properties [10,41,42]. Thus, detailed chemical characterization and scientific understanding of aerosol sources, characteristics, and transformation processes are crucial for quantitative evaluation, credible projections, and viable air pollution control. Various source apportionment (SA) methodologies were utilized to estimate the source contributions. Receptor models (RMs) such as principal component analysis (PCA)/absolute principal component scores (APCS), UNMIX, and positive matrix factorization (PMF) have been used in recent SA investigations on PM sources. The literature summarizes these RMs and their benefits [43–46].

The Himalayas have a substantial regional to global role in meteorology and climate, and is considered an essential and intricate environment from a dynamic atmospheric circulation perspective [20]. The valley breeze processes on the Himalayan slopes can transmit aerosol-enriched boundary layer air to the higher elevations, which is presents a cause for concern regarding the melting glaciers that have been documented throughout the Himalayas [47,48]. Several studies on aerosol chemical compositions have been conducted over the Tibetan Plateau [49–55], in the northern part of the Himalayas, and over the Indian plains [10,56–60]. In contrast, the Indian Himalayan region (IHR) still lacks systematic studies focused on the characterization of aerosols [61–69] and source apportionment [61,70,71] using RMs.

Because of all of the above reasons and the need to understand the sources of PM_{10} over the IHR, this study was designed for SA. This work presents the extension of the previously published research [72], including WSII$_S$, neutralizing reactions of secondary

inorganic aerosols, meteorological parameters, and other chemical components for SA of PM_{10} using different RMs to refine PM_{10} sources over the IHR.

2. Methodology

2.1. Experimental Sites

Diverse observational sites (i.e., Darjeeling, Mohal-Kullu, and Nainital) were selected to represent the IHR which epitomize the eastern, western, and central regions of the Himalayas, respectively (Figure 1). The locations were selected to reflect typical suburban environments. Polluted air originates locally and travels across the transboundary, reaching these sites.
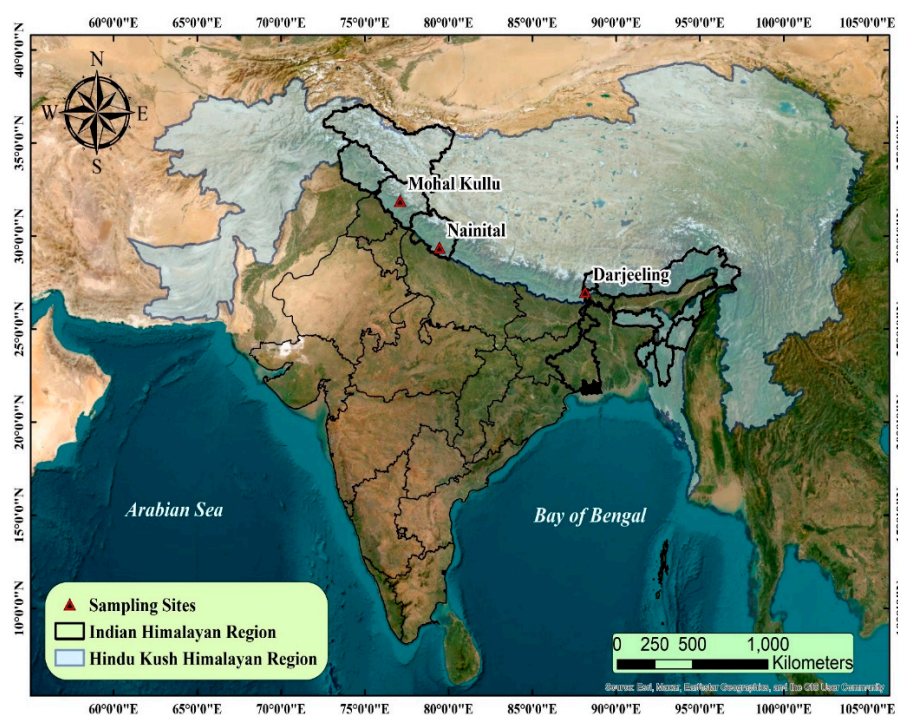
Figure 1. Topographical map showing sampling locations at high altitudes of the Himalayas.

Mohal-Kullu: The G.B. Pant National Institute of Himalayan Environment (NIHE), Mohal-Kullu, is situated in the Kullu Valley at 77.11° E, 31.9° N, and 1154 m above sea level (a.s.l). Great Himalayan ranges from all sides enclose the Kullu Valley. The site now receives snow and rain in the winter (January–February). During summer, the characteristics of aerosols are influenced by air masses from the western side. Detailed information on the sampling site is available in the literature [72,73].

Nainital: The Aryabhatta Research Institute of Observational Sciences (ARIES), Manora peak hill, in Nainital (79.45° E, 29.39° N, 1958 m a.s.l), is a high-altitude location in the IHR. The sampling site is flanked to the northeast by forests and high-altitude ranges and gradually merges with low-altitude plain regions and the Indo-Gangetic basin to the southwest. The site is expected to be emblematic of local and regional environments for climatic change studies [37,74,75]. Additional details about the location are available in the literature [71,72,76].

Darjeeling: The Bose Institute, Darjeeling, was selected to study the characteristics of aerosols (88.15° E, 27.01° N, 2200 m a.s.l.). Darjeeling is a renowned tourist destination with a broad array of altitudinal changes from 300–3500 m in the eastern Himalayan region. Due to its altitudinal variations, the Darjeeling Himalaya exhibits climatic quirks, significantly impacting airflow, precipitation, and temperature [62]. It has the typical monsoon weather, with rainy summers and dry winters. Significant exposure to the moist southwest monsoon emanating from the Bay of Bengal from June to September causes the wet monsoon climatic

condition. The sampling site is situated 200 m above the city level in an area forested with thick vegetation. Many hotels, market complexes, and tea estates are located within 10 to 15 km of the location, resulting in heavy foot traffic [72]. The literature provides additional details about the Darjeeling region [62,72,77,78].

2.2. Sampling and Chemical Analysis

PM_{10} samples were collected periodically at sampling sites from August 2018 to December 2019. Before sampling, Pallflex quartz micro-fiber filters (M/s. PALL Life Sciences, Port Washington, NY, USA) were baked at a high temperature of 550 °C for 5 h using the furnace to eradicate all organic impurities from the filter. The collection of PM_{10} samples was conducted by a high-volume (average flow rate = 1.12 m^3 min^{-1}) respirable dust sampler (M/s. Envirotech, Delhi, India), with an accuracy of $\pm$ 2%. Before and after collection, a microbalance with a resolution of ± 10 µg was used to weigh the filters. Detailed information in the context of the sampling procedure is available in the literature [64,72].

The OC and EC concentrations of each PM_{10} filter were analyzed using an OC/EC Carbon Analyzer (Model: DRI 2001A, Atmoslytic Inc., Calabasas, CA, USA). The detailed analytical procedure for OC/EC estimation is explained in Chow et al. [79]. Non-destructive quantitative estimation of heavy and trace elements was carried out using wavelength dispersive X-ray fluorescence (WD-XRF) (Model: Rigaku ZSX Primus, with an analytical error of 5–10%). For water-soluble organic carbon (WSOC), a TOC analyzer (Model: TOC LCPH/CPN, M/s. Shimadzu, Kyoto, Japan) was used. The MDL of all the measured samples was ≤ 0.1 µg C m^{-3}. The details of the principle and analytical procedures of OC/EC, WSOC, and element analysis are explained in our other publications [26,72].

The $WSII_S$ of PM_{10} were analyzed using the Metrohm 930 compact Ion Chromatography (IC) flex (M/s. Metrohm, Herisau, Switzerland). An IC system was used consisting of a conductivity detector, a suppressor, a cation (Metrosep C 4-150/4.0), and an anion (Metrosep A Supp 5-250/4.0) column. Laboratory analysis is detailed elsewhere [80,81].

2.3. Source Identification Using PCA/APCS, UNMIX, and PMF

2.3.1. Principal Component Analysis/Absolute Principal Component Scores (PCA/APCS)

PCA is a multivariate statistical tool that reduces the complexity of large datasets to the minimum possible components based on their variance using varimax rotation [82] to make the data more interpretable. The orthogonal transformation method was employed to transform correlated variables of the high-dimension matrix into independent components [83,84] to reform intercorrelated variables. Here, PCA/APCS was used by IBM SPSS version 26 to analyze PM_{10} data in order to identify their sources.

Accordingly, the first step in the PCA was to standardize the dataset into a non-dimensional form as an equation:

$$S_{ij} = \frac{C_{ij} - C_j}{\sigma_j} \tag{1}$$

where *i* = no. of samples; *j* = no. of elements in a sample; C_{ij} = *j*th element concentration in sample *i*; C_j = mean concentration of element *j*; and σ_j= standard deviation of element *j*.

After standardization, the PCA illuminates the chemical mass balance as

$$S_{ij} = \sum_{k=1}^{p} g_{ik} h_{kj} \tag{2}$$

where g_{ik} and h_{kj} are the factor loadings and scores, respectively; *k* = *p* no. of sources. Equation (3) is solved by eigenvector decomposition. Only the components having eigenvalues >1 were included as principal components (PC). After the PCs, true zero

was calculated for each factor score and referred to as absolute principal component scores (APCS). These scores were coupled to linear regression using the equation:

$$M = \sum_{k=1}^{n} c_k \times APCS_k \qquad (3)$$

where M = the measured mass concentration; C_k = the unaccounted mass contribution of sources in PCA; and $APCS_k$ = rotated absolute PC scores for each source in a sample.

Therefore, for predicting the modeled mass concentration corresponding to each species for a contribution of estimated sources, the regression coefficient is multiplied by APCS. Detailed explanations of model algorithms are available in the literature [82,84–88].

2.3.2. UNMIX

UNMIX is a multivariate model having non-negativity constraints. In the UNMIX model (US EPA UNMIX 6.0), the number of sources is estimated using the singular value decomposition method (SVD method). In the SVD method, the dimensionality of data is reduced to find the edge points. Edge points refer to specific data points where one source's contribution is negligible compared with others. UNMIX locates these edge points and creates a hyperplane through them, called an edge. Thus, these hyperplanes provide source compositions, and the source contributions are calculated to best fit the data. An in-depth explanation of the model and algorithms are available in the literature [27,89–91].

2.3.3. Positive Matrix Factorization (PMF)

The US EPA PMF (version 5.0) is a multivariate receptor tool for factor analysis. The PMF model extracts factor contributions (G) and factor profiles (H) from a sample data matrix. PMF requires two types of files: a species concentration file and a species uncertainty file. The standard equation-based uncertainty (U) is formulated as an equation

$$U = \sqrt{(ef * C)^2 + (0.5 \times MDL)^2} \qquad (4)$$

where ef is the error fraction, C is the concentration, and MDL is the method detection limit of species. For each species, the signal/noise ratio (S/N) represents the measurement heterogeneity (i.e., absolute measurement or within the noise measurement).

A PMF primary output of contribution and profile is obtained from the initial model base run. Q_{value} (goodness of fit parameter), i.e., how well the input and model data match, was clarified by interpretation of the outcomes of the base model run. Q_{robust} (goodness of fit parameter discarding the values with uncertainty-scaled residual > 4) data show the fitness of the runs compared with Q_{true} (goodness of fit parameter considering all points). The user can obtain the global minimum by analyzing the strength of Q_{robust} and random seeds. Species with large residual values are a poor fitting indicator; thus, a residual value of -3 to $+3$ is preferred, corresponding to a normal distribution (EPA PMF User guide, 2014).

DISP, BS, and BS-DISP are three methods that can be used to estimate errors. In contrast to the BS interval, which accepts random errors in judgement and some rotational discrepancy, DISP considers rotational discrepancy. The DISP intervals are affected by incorrect user specification of data uncertainty; however, the BS interval is not affected by incorrect user specification. Although the BS-DISP misspecifies data uncertainty, it can accommodate rotational uncertainties and random errors [92–95].

In this investigation, we employed PMF version 5.0. The PMF model scrutinizes the input and equation-based uncertainty data files to comprehend the sources and percentage profile. In the present scenario, the input data file includes the carbonaceous carbon (EC, OC, and WSOC), elemental composition (Al, Cr, Ti, Mn, Fe, Zn, Cu, Br, Mo, Pb, and Ba), and the WSIIS (F^-, Cl^-, SO_4^{2-}, NO_3^-, Na^+, NH_4^+, K^+, Mg^{2+}, and Ca^{2+}). The equation-based uncertainty was calculated using Equation (4), corresponding to the input speciated data.

Table S1 (Supplementary Materials) shows the MDL used for the three sites' uncertainty calculations and signal-to-noise ratios. Tables S2–S4 (Supplementary Materials) summarize the PMF-model measures for the present study sites. Sources were resolved at study sites by incorporating the model data (S/N, R^2, time series) with the base model and error estimation. Species with an S/N ratio < 0.5 are considered bad, 0.5–1 are weak, and >1 are strong species.

2.3.4. Meteorological Data and Backward Trajectory Analysis

Meteorological data, such as relative humidity (RH) (accuracy $\pm$ 2%), temperature (T) (accuracy $\pm$ 1 °C), wind speed (WS) (accuracy $\pm$ 2% of full scale), and wind direction (WD) (accuracy $\pm$ 3°) were collected using the automatic weather stations (AWS) at sampling sites during the study period (2018–2019). Backward air mass trajectories were generated using an HYSPLIT model by employing GDAS global meteorological data to examine the long-range and regional transport of aerosols to study regions, namely, Mohal-Kullu, Nainital, and Darjeeling. Seasonal air mass back trajectories of 72 h were considered at 500 m above ground level (AGL) for each sampling day (August 2018–December 2019).

3. Results

In this section, we infer the predominant aerosol phenomenon in the IHR in terms of their possible origins, atmospheric processes, and transit from PM_{10}, along with its carbonaceous, elemental, and WSIIS compositions and diagnostic ratios as a function of seasons. We then qualitatively and quantitatively analyze the role of chemical and meteorological factors in regulating aerosol acidity. Lastly, RMs quantify PM_{10} sources over the IHR.

3.1. Potential Sources, Atmospheric Processes, and Transport of PM_{10} in the IHR

This paper reports variations in WSIIS and assesses PM_{10} sources using different RMs and their model inter-comparisons for source identification; our previous paper [72] discussed the concentrations and seasonality of carbonaceous components and trace and heavy elements of PM_{10}.

3.1.1. Variations in PM_{10} Mass and Its Chemical Composition

Table 1 summarizes the measured chemical species' annual and seasonal mean concentrations in PM_{10}. The highest yearly average concentration of PM_{10} was observed at Nainital (62 $\pm$ 39 μg m^{-3}), followed by Mohal Kullu (58 $\pm$ 32 μg m^{-3}) and Darjeeling (54 $\pm$ 18 μg m^{-3}) (Figure S1), which are higher than the WHO permissible limit (15 μg m^{-3}) and near (annual: 60 μg m^{-3}) the National Ambient Air Quality Standards (NAAQS) of India. The temporal variation in PM_{10} concentration with meteorological parameters such as T, WS, RH, and WD are represented in Figure 2. Seasons were classified according to the Indian Meteorological Department (IMD) seasonal classification as winter (January–February), summer (March–May), monsoon (June–September), and post-monsoon (October–December). Figure S1 (Supplementary Materials) reported the seasonal concentration of PM_{10} at different study sites. Over Nainital, the highest concentration of PM_{10} was observed in summer, followed by post-monsoon, monsoon, and winter, which might be due to the high wind speed (Figure 2) in summer being responsible for airflow of dust-related pollutants from the IGP and nearby regions. Darjeeling experiences the highest concentration of PM_{10} in the summer, followed by winter, post-monsoon, and the minimum in the monsoon season. Compared with other sites, a sharp decrease in the concentration of PM_{10} was not observed over Darjeeling in the monsoon season due to the enhanced contribution of sea salt aerosol species (Na$^+$, Cl$^-$, Mg^{2+}, non-sea-salt sulfate, and nitrate).

Table 1. The annual and seasonal average concentrations of PM_{10} and their carbonaceous components (OC, EC, WSOC, and WSIC) at different study sites of the IHR.

All Units Are in µg m^{-3}	Annual (August 2018–December 2019)	Winter (January–February)	Summer (March–May)	Monsoon (June–September)	Post Monsoon (October–December)
Darjeeling					
No. of Samples (n)	n = 134	n = 25	n = 32	n = 31	n = 46
PM_{10}	54 ± 18	52 ± 18	63 ± 21	47 ± 9	50 ± 15
OC	5.13 ± 2.33	5.43 ± 2.02	5.21 ± 2.14	3.11 ± 1.02	6.32 ± 2.41
EC	2.20 ± 1.22	2.72 ± 1.00	3.01 ± 1.15	1.13 ± 0.45	2.12 ± 1.05
WSOC	3.61 ± 1.91	3.92 ± 1.31	3.43 ± 2.22	1.82 ± 0.91	4.71 ± 1.61
POC	2.90 ± 1.51	3.54 ± 1.30	3.91 ± 1.53	1.70 ± 0.60	3.22 ± 1.44
SOC	2.33 ± 1.52	1.94 ± 1.14	1.32 ± 1.05	1.42 ± 0.91	3.11 ± 1.53
TCA	10.41 ± 4.74	13.04 ± 4.71	13.11 ± 5.20	6.62 ± 1.93	13.52 ± 5.14
Na^+	1.46 ± 0.88	1.43 ± 0.73	1.97 ± 1.22	1.14 ± 0.48	1.33 ± 0.72
NH_4^+	2.88 ± 3.40	3.99 ± 4.11	4.73 ± 4.30	1.57 ± 1.75	1.91 ± 2.29
K^+	0.61 ± 0.46	0.63 ± 0.37	0.76 ± 0.50	0.25 ± 0.18	0.72 ± 0.48
Mg^{2+}	0.13 ± 0.16	0.11 ± 0.10	0.23 ± 0.26	0.08 ± 0.07	0.10 ± 0.10
Ca^{2+}	0.69 ± 0.62	0.61 ± 0.25	1.15 ± 1.02	0.46 ± 0.27	0.54 ± 0.33
F^-	0.04 ± 0.08	0.03 ± 0.05	0.08 ± 0.15	0.02 ± 0.01	0.03 ± 0.02
Cl^-	0.55 ± 0.74	0.36 ± 0.20	1.01 ± 1.31	0.35 ± 0.26	0.47 ± 0.40
NO_3^-	2.29 ± 2.52	2.43 ± 2.47	3.66 ± 3.77	1.09 ± 1.12	2.06 ± 1.73
SO_4^{2-}	5.36 ± 5.49	5.90 ± 5.22	8.43 ± 8.11	3.83 ± 3.50	3.96 ± 3.22
Nainital					
No. of Samples (n)	n = 86	n = 17	n = 27	n = 9	n = 33
PM_{10}	62 ± 39	38 ± 9	100 ± 50	49 ± 17	47 ± 14
OC	5.31 ± 4.60	2.90 ± 1.05	8.30 ± 7.15	4.32 ± 1.70	4.31 ± 1.33
EC	1.70 ± 1.12	1.32 ± 0.61	2.31 ± 1.43	1.45 ± 0.81	1.42 ± 0.84
WSOC	3.67 ± 2.70	2.11 ± 0.60	5.71 ± 3.45	3.20 ± 1.40	3.01 ± 1.71
POC	2.71 ± 1.71	2.33 ± 1.05	3.74 ± 2.32	2.80 ± 1.43	2.54 ± 1.32
SOC	2.63 ± 3.51	0.74 ± 0.34	4.74 ± 5.62	1.55 ± 1.20	1.83 ± 1.22
TCA	11.10 ± 8.74	6.71 ± 2.45	16.94 ± 13.25	9.24 ± 3.52	9.13 ± 2.95
Na^+	0.44 ± 0.40	0.23 ± 0.12	0.63 ± 0.50	0.45 ± 0.46	0.40 ± 0.33
NH_4^+	1.80 ± 0.98	1.06 ± 0.64	2.12 ± 0.78	2.11 ± 1.18	1.82 ± 1.06
K^+	0.46 ± 0.28	0.30 ± 0.15	0.60 ± 0.38	0.50 ± 0.13	0.40 ± 0.20
Mg^{2+}	0.10 ± 0.08	0.06 ± 0.02	0.13 ± 0.06	0.14 ± 0.08	0.09 ± 0.07
Ca^{2+}	0.90 ± 0.93	0.46 ± 0.26	1.25 ± 1.37	1.12 ± 0.78	0.77 ± 0.58
F^-	0.04 ± 0.02	0.04 ± 0.02	0.04 ± 0.02	0.04 ± 0.03	0.03 ± 0.02
Cl^-	0.31 ± 0.37	0.23 ± 0.18	0.50 ± 0.56	0.17 ± 0.10	0.24 ± 0.21
NO_3^-	2.12 ± 1.23	1.32 ± 0.80	2.63 ± 1.24	2.44 ± 1.57	1.89 ± 1.03
SO_4^{2-}	4.04 ± 2.01	2.39 ± 0.78	4.95 ± 1.53	4.63 ± 2.41	3.69 ± 1.80
Mohal-Kullu					
No. of Samples (n)	n = 76	n = 5	n = 8	n = 34	n = 29
PM_{10}	58 ± 32	51 ± 16	52 ± 15	44 ± 26	76 ± 36
OC	10.71 ± 8.25	11.14 ± 5.33	11.50 ± 6.21	6.54 ± 4.65	15.43 ± 9.95
EC	3.50 ± 2.05	4.23 ± 1.91	3.75 ± 1.54	2.35 ± 1.31	4.70 ± 2.05
WSOC	5.55 ± 3.24	5.32 ± 1.26	4.30 ± 3.00	4.24 ± 1.65	7.50 ± 4.11
POC	6.82 ± 3.92	9.30 ± 4.21	7.20 ± 2.94	4.80 ± 2.64	9.11 ± 4.04
SOC	3.94 ± 4.90	1.84 ± 1.65	4.31 ± 3.44	1.81 ± 2.43	6.33 ± 6.51
TCA	20.71 ± 15.10	22.05 ± 10.34	22.05 ± 11.44	12.82 ± 8.70	29.36 ± 17.84
Na^+	2.63 ± 2.11	2.18 ± 0.73	1.81 ± 0.32	2.23 ± 1.89	3.41 ± 1.22
NH_4^+	1.88 ± 1.50	1.61 ± 0.90	1.01 ± 0.50	1.50 ± 1.20	2.61 ± 1.78
K^+	0.55 ± 0.51	0.40 ± 0.17	0.39 ± 0.42	0.38 ± 0.38	0.82 ± 0.61
Mg^{2+}	0.26 ± 0.21	0.39 ± 0.34	0.11 ± 0.11	0.31 ± 0.28	0.20 ± 0.23
Ca^{2+}	1.47 ± 1.22	1.66 ± 0.75	1.03 ± 0.36	1.07 ± 0.91	2.04 ± 1.51
F^-	0.10 ± 0.07	0.08 ± 0.02	0.05 ± 0.03	0.09 ± 0.07	0.12 ± 0.07
Cl^-	1.76 ± 1.11	1.66 ± 0.79	1.00 ± 0.23	1.40 ± 0.87	2.41 ± 1.25
NO_3^-	2.45 ± 1.67	2.31 ± 0.97	1.53 ± 0.57	1.98 ± 1.18	3.28 ± 2.11
SO_4^{2-}	2.65 ± 1.75	2.51 ± 1.17	1.58 ± 0.58	2.31 ± 1.46	3.43 ± 2.07
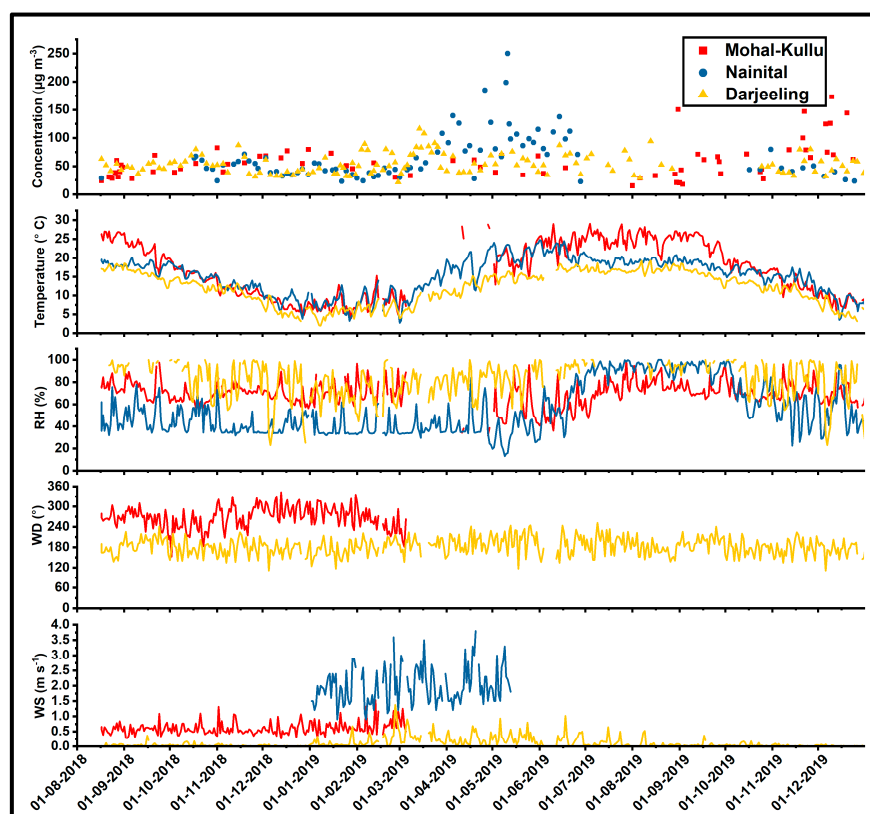
Figure 2. Temporal variation in PM_{10} concentration and meteorological parameters during the study period over high-altitude sites of the IHR.

Figure S2 (Supplementary Materials) shows the average seasonal concentration of CAs estimated at the study sites. The observation sites experience enhanced concentrations of carbonaceous components in the winter/post-monsoon [72] seasons, which might be due to meteorological factors such as shallow mixing height, low WS, and temperature (Figure 2), favoring stagnant weather conditions. In addition, other factors such as massive biomass burning (BB) activities, traffic congestion, and residential burning increased the load of particulate CAs over the study sites [71,72,77,78]. Volatilization of CAs and airflow of contaminants from the IGP northwest region due to stubble burning activities after crop harvesting resulted in high CA concentrations at high altitude sites during summer [4,26,66,96–100]. Figure S3 (Supplementary Materials) shows the percentage contribution of OC, EC, WSOC, trace, heavy elements, and WSIIS of PM_{10} at the observation sites.

The estimated trace elements constituted around 18%, 15%, and 9% of PM_{10} at the Mohal-Kullu, Nainital, and Darjeeling study sites. Overall, the average concentration of crustal components (Ca, Al, Fe, K, and Na) was considerably higher at all study sites (Mohal-Kullu: 5.61 ± 3.44 µg m^{-3}, Nainital: 7.14 ± 6.28 µg m^{-3}, and Darjeeling: 2.94 ± 2.27 µg m^{-3}), while other elements have significant elemental concentrations in PM_{10} [72]. Table S5 (Supplementary Materials) shows the annual and seasonal average concentrations of trace and heavy elements in PM_{10} over the study sites. On average, the highest crustal elemental concentration observed in the summer season might be due to long-range dust transport from arid regions and construction activities resulting in coarse-mode crustal components at study sites. A substantial positive correlation of Al with Mg, Ca, Ti, and Fe (Figure S4) (Supplementary Materials) reflects the abundance of mineral/crustal dust as a source of PM_{10} over the study sites.

3.1.2. Variation in Water-Soluble Inorganic Ionic Species (WSIIS) of PM_{10}

PM_{10} samples were analyzed for major anions and cations. Table 1 illustrates the seasonal and annual average WSIIS concentrations at three sampling sites. The annual total WSIIS concentration order was as follows: Darjeeling ($14.02 \pm 10.01\ \mu g\ m^{-3}$) > Mohal-Kullu ($13.75 \pm 10.21\ \mu g\ m^{-3}$) > Nainital ($10.20 \pm 6.30\ \mu g\ m^{-3}$), contributing to 15–30% of the PM_{10} mass as shown in Table 1. Regarding mass percentage loading of WSIIS, the order of cations was as follows: NH_4^+ > Na^+ > Ca^{2+} > K^+ > Mg^{2+}. The SO_4^{2-} anion followed by NO_3^- and Cl^- predominated at all sampling sites due to secondary production from precursor gases and transformation rates (Figures 3–5) [52,101,102]. The major secondary ions (NH_4^+, SO_4^{2-}, and NO_3^-) indicated that long-range and regional transport of anthropogenic sources significantly influence the study sites [103,104].
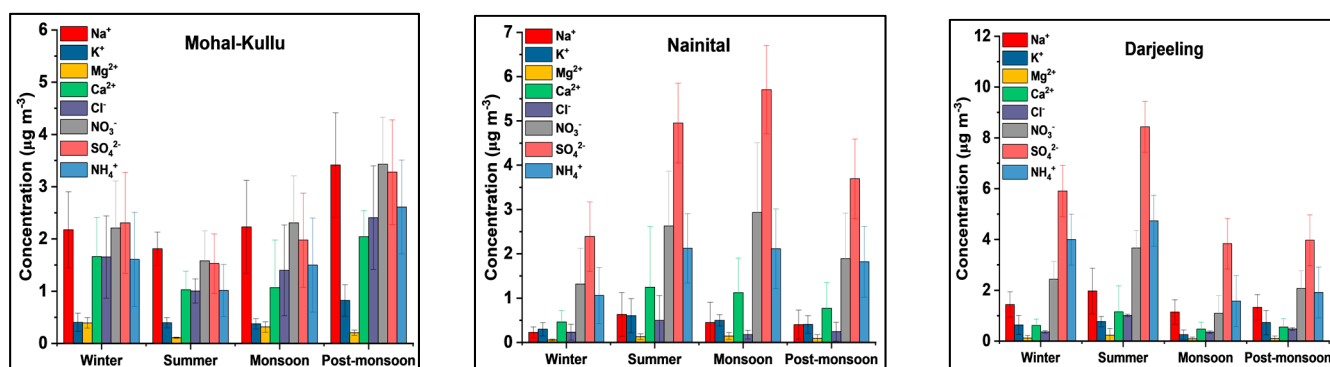
Figure 3. Seasonal average contributions of water-soluble inorganic ionic species (WSIIS) of PM_{10} at the different study sites.

The primary $WSII_S$ (Ca^{2+}, Mg^{2+}, K^+, Na^+, and Cl^-) over Nainital show higher Na^+ and Cl^- concentrations in the summer, followed by the winter, post-monsoon, and monsoon seasons. The Nainital site is not influenced by marine air masses [71,105]. During summer, dust aerosols might contribute to Na^+, which can react heterogeneously with acidic gases and form water-soluble Na^+ [80]. Whereas Cl^- might be due to a forest fire near the site and the long-range transport of aerosols. Our findings infer that the concentration of Na^+ and Cl^- in the monsoon season might be due to the transport of marine air masses from the BoB (Figure 6). Strong seasonal variations in Na^+ and Cl^- concentrations were observed in the monsoon season over Darjeeling [62]. The results from the Darjeeling site show that Cl^- reached its maximum peak during summer followed by winter, and post-monsoon could be associated with coal burning in Darjeeling railways, transport of anthropogenic aerosols, use of fertilizers, and enhanced tourist activities [61,62]. Ca^{2+} and Mg^{2+} are primary crustal sources showing higher concentrations during summer, possibly due to long-range transport and low precipitation favorable for the re-suspension of wind-blown soil dust (SD) particles [49,106] to the study sites. The highest concentration of K^+ was observed in the post-monsoon season (Table 1), which might be due to plumes of crop residue burning in the IGP (Figure 6) being transported to higher altitudes. The peak of K^+ in winter is due to enhanced wood/coal burning activities caused by meteorological conditions (Figure 2), while in summer it is due to the regional transport of pollutants (Figure 6) over the study sites [61,62,71,107,108].

Among the Secondary WSIIS (SO_4^{2-}, NO_3^-, and NH_4^+), the SO_4^{2-} ion was the predominant one at the study sites. Over Darjeeling, the maximum SO_4^{2-} concentration was observed during the summer ($8.43 \pm 8.41\ \mu g\ m^{-3}$) and winter ($5.90 \pm 5.22\ \mu g\ m^{-3}$), followed by the post-monsoon season ($3.96 \pm 3.22\ \mu g\ m^{-3}$), and the minimum concentration was observed in the monsoon season ($3.83 \pm 3.50\ \mu g\ m^{-3}$) (Figure 3). Whereas in the case of Nainital, the summer months ($4.95 \pm 1.53\ \mu g\ m^{-3}$) reported a high concentration of SO_4^{2-}, followed by the monsoon, post-monsoon, and winter seasons. During summer, high temperature (Figure 2) and intense solar radiation (SR) enhanced the gas phase photochemical

oxidation of SO$_2$ along with the advected pollution plume of the IGP (Figure 6) and local combustion-related activities resulting in elevated SO$_4^{2-}$ concentrations in summer over Darjeeling and Nainital. Ghosh et al. [62] also reported high concentrations of SO$_4^{2-}$ in summer due to the photochemical oxidation of SO$_2$. In contrast, over Mohal-Kullu, a high concentration of SO$_4^{2-}$ was observed in the post-monsoon season (3.43 ± 2.07 μg m^{-3}), followed by the winter (2.51 ± 1.17 μg m^{-3}), monsoon, and summer seasons. During the post-monsoon season, heterogeneous conversion of SO$_2$ to SO$_4^{2-}$ aerosols increases under favorable meteorological conditions (low WS, T, and mixing height). The high concentration of SO$_4^{2-}$ during the winter season at the study sites might be due to increased emissions from combustion activities and residential burning for domestic purposes and prevailing atmospheric conditions (Figure 2) [62] (Table 1).

Mohal-Kullu

	OC	EC	WSOC	Na$^+$	NH$_4^+$	K$^+$	Mg^{2+}	Ca^{2+}	F$^-$	Cl$^-$	NO$_3^-$	SO$_4^{2-}$
OC	1.0											
EC	0.93	1.0										
WSOC	0.65	0.60	1.0									
Na$^+$	0.75	0.62	0.55	1.0								
NH$_4^+$	0.63	0.58	0.39	0.48	1.0							
K$^+$	0.80	0.68	0.51	0.71	0.61	1.0						
Mg^{2+}	0.033	-0.029	-0.037	0.019	-0.072	0.14	1.0					
Ca^{2+}	0.76	0.66	0.54	0.69	0.57	0.82	0.18	1.0				
F$^-$	0.50	0.39	0.46	0.53	0.40	0.65	0.13	0.68	1.0			
Cl$^-$	0.66	0.56	0.50	0.70	0.56	0.82	0.085	0.80	0.70	1.0		
NO$_3^-$	0.69	0.61	0.44	0.54	0.95	0.71	-0.0078	0.68	0.53	0.66	1.0	
SO$_4^{2-}$	0.63	0.58	0.40	0.52	0.95	0.64	-0.033	0.63	0.51	0.62	0.94	1.0

Nainital

	OC	EC	WSOC	Na$^+$	NH$_4^+$	K$^+$	Mg^{2+}	Ca^{2+}	F$^-$	Cl$^-$	NO$_3^-$	SO$_4^{2-}$
OC	1.0											
EC	0.75	1.0										
WSOC	0.90	0.80	1.0									
Na$^+$	0.24	0.20	0.31	1.0								
NH$_4^+$	0.46	0.49	0.55	0.19	1.0							
K$^+$	0.85	0.62	0.80	0.24	0.58	1.0						
Mg^{2+}	0.47	0.31	0.45	0.33	0.38	0.53	1.0					
Ca^{2+}	0.12	0.050	0.13	0.27	0.31	0.042	0.44	1.0				
F$^-$	-0.031	-0.017	0.026	0.13	-0.19	-0.12	0.057	0.24	1.0			
Cl$^-$	0.45	0.13	0.43	0.32	0.25	0.46	0.29	0.42	0.30	1.0		
NO$_3^-$	0.55	0.53	0.62	0.16	0.91	0.64	0.58	0.32	-0.12	0.27	1.0	
SO$_4^{2-}$	0.42	0.43	0.53	0.24	0.85	0.55	0.50	0.29	-0.21	0.17	0.88	1.0

Darjeeling

	OC	EC	WSOC	Na$^+$	NH$_4^+$	K$^+$	Mg^{2+}	Ca^{2+}	F$^-$	Cl$^-$	NO$_3^-$	SO$_4^{2-}$
OC	1.0											
EC	0.76	1.0										
WSOC	0.86	0.69	1.0									
Na$^+$	0.13	0.24	0.077	1.0								
NH$_4^+$	0.40	0.58	0.37	0.11	1.0							
K$^+$	0.77	0.69	0.66	0.15	0.48	1.0						
Mg^{2+}	0.29	0.42	0.28	0.21	0.58	0.49	1.0					
Ca^{2+}	0.33	0.45	0.32	0.23	0.54	0.47	0.64	1.0				
F$^-$	0.32	0.36	0.31	0.13	0.58	0.45	0.77	0.61	1.0			
Cl$^-$	0.36	0.45	0.38	0.13	0.61	0.51	0.76	0.81	0.77	1.0		
NO$_3^-$	0.44	0.54	0.41	0.12	0.88	0.55	0.61	0.59	0.58	0.70	1.0	
SO$_4^{2-}$	0.39	0.54	0.37	0.099	0.92	0.47	0.61	0.57	0.61	0.64	0.86	1.0

Figure 4. Pearson correlation coefficients of carbonaceous and WSII species at the different study sites during the study period.
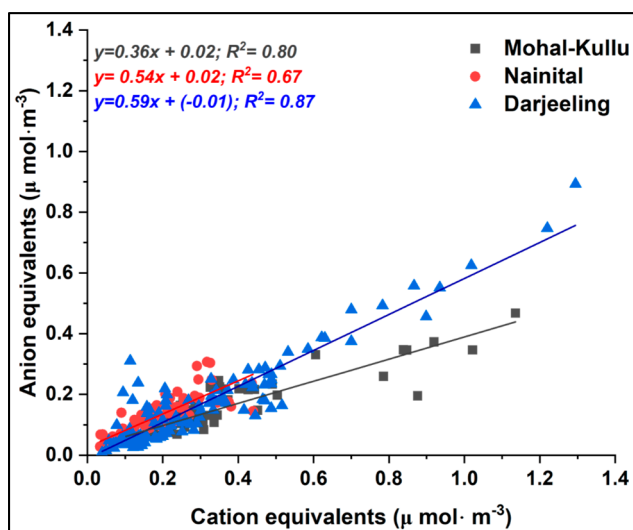
Figure 5. Annual CE/AE ratio for aerosol acidity at the study sites.
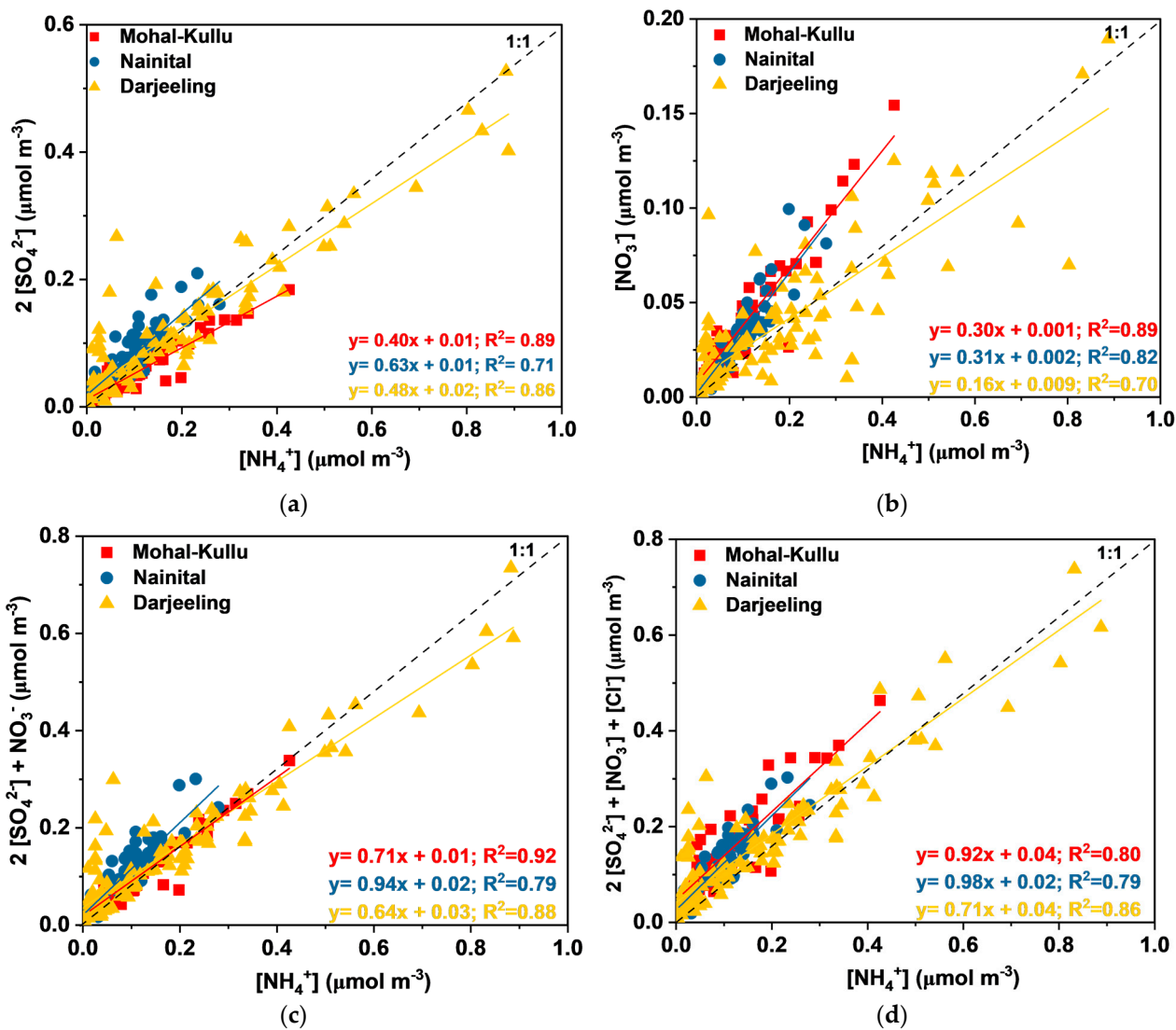
Figure 6. Charge balance (**a**) $2[SO_4^{2-}]/[NH_4^+]$, (**b**) $[NO_3^-]/[NH_4^+]$, (**c**) $2[SO_4^{2-}]+[NO_3^-]/[NH_4^+]$, and (**d**) $2[SO_4^{2-}]+[NO_3^-]+[Cl^-]/[NH_4^+]$ at the different study sites.

NH_4^+ followed seasonal patterns similar to SO_4^{2-} at all study sites, which might indicate the possible existence of NH_4HSO_4 or $(NH_4)_2SO_4$ in the atmosphere. NH_4^+ formed from NH_3 via gas and aqueous phase interactions with acidic species such as HNO_3, HCl, and H_2SO_4 (detailed in subsequent sections). Farming, livestock, combustion, incineration, and BB activities produce NH_3 in the atmosphere. During summer, enhanced combustion activities, BB-transported plumes from the IGP, local anthropogenic activities, and favorable climatic conditions increased the NH_4^+ concentration over Nainital and Darjeeling. In contrast, over Mohal-Kullu, a high concentration of NH_4^+ in the post-monsoon and winter seasons might be due to an enhanced NH_3 from local and advected burning plumes that could expedite the heterogeneous conversion of NH_3 to NH_4^+ [109].

Over Darjeeling and Nainital, the peak of NO_3^- observed in summer might be due to enhanced vehicular activities and gas phase conversion of NO_2 to HNO_3 by OH radicals [61,62,110]. During the summer, conditions such as high SR and T and low RH partially decompose NH_4NO_3. In contrast, during the winter and post-monsoon seasons, aqueous phase conversion of NO_2 to NO_3 occurs, and HNO_3 reacts with NH_3 to form NH_4NO_3 [19,62,101,109–111]. Similar seasonal patterns of SO_4^{2-} and NO_3^- were also reported in several research articles [4,61,62,109,112–117].

3.1.3. Correlation of Carbonaceous and WSIIS of PM_{10}

Studying correlations among carbonaceous and WSIIS mass concentrations and diagnostic ratios is an appropriate way to identify potential PM sources. Figure 4 shows the annual Pearson correlation of CAs and WSIIS at the study sites.

Table S6 reports the seasonal and annual diagnostic mass concentration ratios of carbonaceous species and WSIIS over the study sites. Several earlier studies considered non-sea-salt K^+ (nssK^+) (calculated as $K^+ = 0.129Na^+$) as a tracer for BB along with CAs [46,79,118]. The values of nssK^+/EC in Nainital (0.31) and Darjeeling (0.26) propound the BB contributions to EC, which are similar to those reported earlier [62,66,111], while a value of nssK^+/EC less than 0.20 indicates emissions from fossil fuel combustion (FFC) as shown by Mohal-Kullu (0.14). Significant correlation of K^+/EC (r = Mohal-Kullu: 0.68; Nainital: 0.62; and Darjeeling: 0.69), K^+/OC (r = Mohal-Kullu: 0.80; Nainital: 0.85; and Darjeeling: 0.79), K^+/Cl^- (r = Mohal-Kullu: 0.82; Nainital: 0.46; and Darjeeling: 0.52), and K^+/NO_3^- (r = Mohal-Kullu: 0.71; Nainital: 0.64; and Darjeeling: 0.55) may imply their common source of BB at different study sites of the IHR [81,89,110,111,119]. K^+ also originated from crustal source interference, such as re-suspension of soil dust [119]. A significantly high correlation coefficient of K^+ and Ca^{2+} was observed, (r = 0.82, $p < 0.05$) and (r = 0.47), for Mohal-Kullu and Darjeeling, respectively, and the source was determined to be soil re-suspension. The ratio of Mg^{2+}/Ca^{2+} was 0.32, 0.59, and 0.23 at Mohal-Kullu, Nainital, and Darjeeling during the study period, which was higher than the sea salt aerosol ratio (0.18), which reconfirmed that SS was not a significant contributor [19]. At Nainital, Mg^{2+} and Ca^{2+} correlate well (0.77), followed by Darjeeling and Mohal-Kullu in the summer season, likely indicating their communal sources [49,66,106]. SD from surrounding areas and regional transport of dust aerosols (Figure 6) under dry and windy conditions during summer could be the reason for their aerosol enrichment [111] at the study sites. A statistically significant positive correlation of acidic species, such as SO_4^{2-} and NO_3^- with NH_4^+, indicates the production of $(NH_4)_2SO_4$ and NH_4NO_3 to neutralize the acidity of aerosols at the study sites (Figure 5).

3.2. Aerosol Acidity and Charge Balance

Aerosol acidity is a crucial characteristic of atmospheric particulates that affect clouds, climate, ambient quality, and human well-being [120].

Aerosol acidity: $WSII_S$ are important in regulating the acidity of aerosols and their acidification in the environment. Ion balance reactions are good indicators to estimate

the acid–base equilibrium of aerosol particles. Therefore, in the present study, both anion equivalents (*AE*) and cation equivalents (*CE*) are calculated by the following equation:

$$CE = \frac{Na^+}{23} + \frac{NH_4^+}{18} + \frac{K^+}{39} + \frac{Mg^{2+}}{12} + \frac{Ca^{2+}}{20} \tag{5}$$

$$AE = \frac{SO_4^{2-}}{96} + \frac{NO_3^-}{62} + \frac{Cl^-}{35.5} \tag{6}$$

During the study period, the correlation coefficients of CE and AE were in the range of 0.67–0.87, indicating the alkaline nature of aerosol-causing aerosol acidity at the study sites (Figure 5). Seasonal correlations of CE and AE were also reported indicating the acidity of the aerosols at the study sites (Figure S5).

Charge balance: The acidic aerosols (SO_4^{2-} and NO_3^-) can be neutralized by alkaline components such as NH_3 and $CaCO_3$. NH_4^+, Ca^{2+}, and Mg^{2+} are dominant acid-neutralizing cations. During the present study, the equivalent molar ratios of NH_4^+ /SO_4^{2-} and NH_4^+/ NO_3^- were 3.7 and 2.5, 2.8 and 2.6, and 3.0 and 3.8 at Mohal-Kullu, Nainital, and Darjeeling, respectively. These results demonstrate the abundance of NH_4^+ particles to neutralize SO_4^{2-} and NO_3^- particulates and function as a precursor to secondary aerosol formation at the study sites (Figure 6). It was observed that the atmosphere has enough NH_4^+ to neutralize SO_4^{2-} and NO_3^- (preferably 2:1 and 1:1), which was determined by the molar ratio of NH_4^+ to SO_4^{2-} and NO_3^- [97]. Moreover, the complete neutralization of acidic species (HNO_3 and H_2SO_4) by NH_4^+ was calculated using the equivalent ratios of NH_4^+/(NO_3^-+SO_4^{2-}). If the value of NH_4^+/(NO_3^-+SO_4^{2-}) is near 1.0, it implies that the acidity has been completely neutralized by NH_4^+ [121]. The average equivalent ratios of NH_4^+/(NO_3^-+SO_4^{2-}) in PM_{10} from the sampled sites were 1.48, 1.32, and 1.55 at Mohal-Kullu, Nainital, and Darjeeling, respectively, confirming that NH_4^+ plays a significant contribution in acidity neutralization of aerosols over the Himalayas.

3.3. Potential Source Area from the Air Mass Backward Trajectory Analysis

Different air masses travel through different regions, bringing different chemical components of PM to the receptor sites; therefore, air mass flow also sheds some light on their possible source areas and sources. During the study period, air masses at study sites were dominantly southwesterly and northwesterly in summer and winter, respectively, while during the post-monsoon season, a mixture of southwesterly, northeasterly, and northwesterly air masses was observed (Figure 7). During the summer, the enrichment of crustal elements might be due to the long-range transport of dust-related air masses from the IGP, the Thar desert, and windy conditions (Figure 6) at the elevated altitudes as per the elevated-heat-pump mechanism [61]. High concentrations of carbonaceous species and WSIIS in the post-monsoon and winter seasons are attributed to local and transported emissions of BB and fossil fuel combustion, crop residue burning in Punjab and Haryana, and meteorological influences (lowered boundary layer heights and stable atmosphere) (Figure 2) [64,71,76,122,123]. Over Darjeeling, marine air masses from the southeast arriving in the monsoon season are mainly from the Bay of Bengal (BoB) (Figure 6) [62,76], suggesting sea salt aerosols as a source of PM over Darjeeling. Arun et al. [124] reported that the long-range transport over the study site was from northwestern parts of the IGP region, western regions of Asia, and the Middle East. According to Sheoran et al. [71], the major source regions for aerosols in Nainital include Delhi, Punjab, Haryana, Pakistan, the Thar desert (Rajasthan), the Arabian Sea, and East Africa. Rai et al. [64] revealed that the common source regions of PM_{10} over Darjeeling are local areas, the IGP, the Thar desert (Rajasthan), parts of semi-arid and central highlands, and the BoB. Sarkar et al. [125] also reported the IGP and Nepal as the most dominant $PM_{2.5}$ and black carbon (BC) regions.

Winter Season

Summer Season

Monsoon Season

Post-Monsoon Season

Latitude (°)

Longitude (°)

Mohal-Kullu
Nainital
Darjeeling
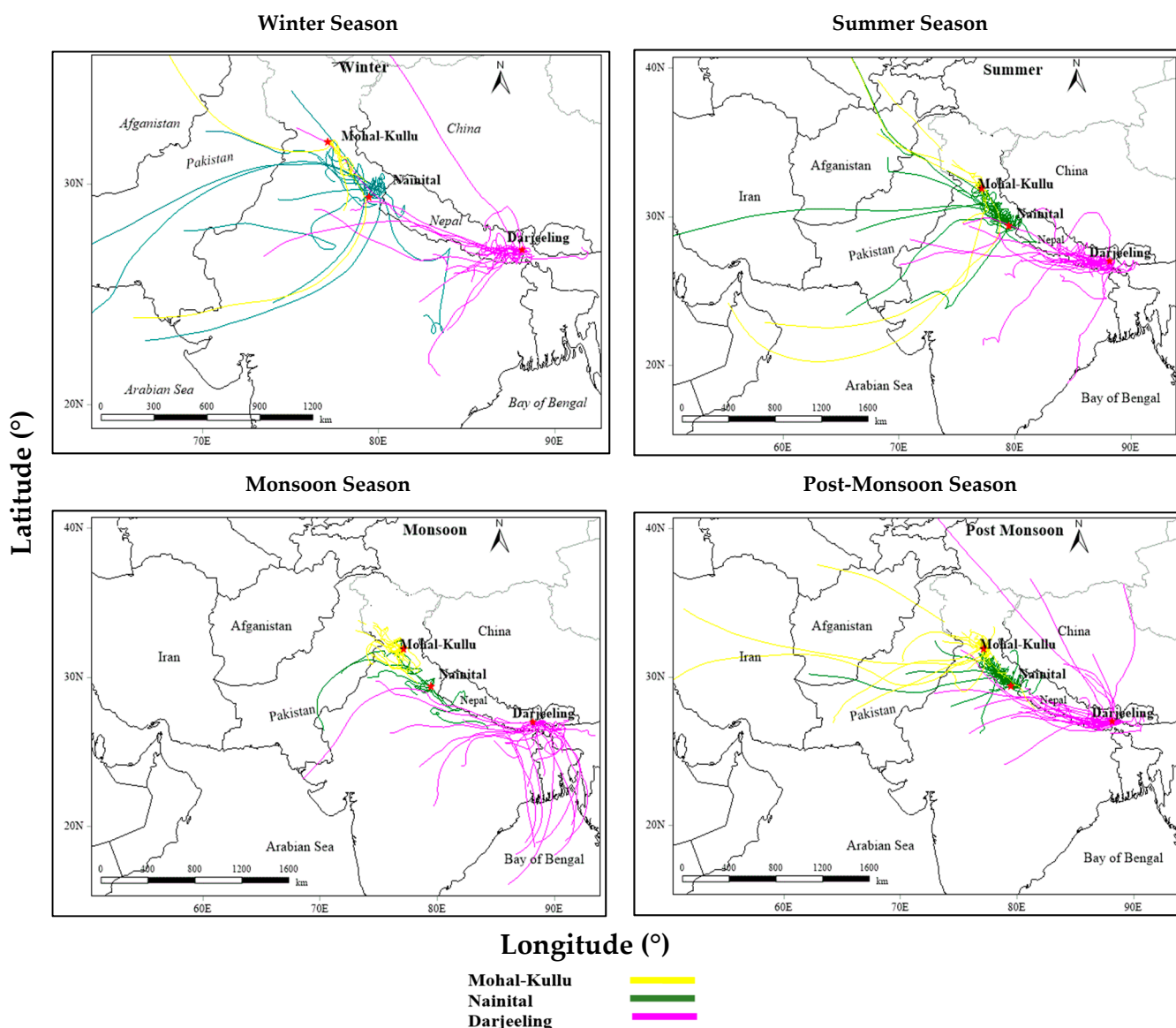
Figure 7. Seasonal air mass backward trajectories at 500 m A.G.L over different high-altitude sites of IHR.

3.4. Source Apportionment of PM$_{10}$ Using Receptor Models

3.4.1. PCA/APCS

PCA/APCS was executed on data of all sites using SPSS software (26.0). In PCA, varimax rotation was applied with orthogonal transformation. Kaiser–Meyer–Olkin (KMO) values were used to measure the adequacy of the model and response suitability. Table S7 shows the factor profiles of the PCA/APCS at the study sites.

Mohal-Kullu

A total of 77 samples and 18 chemical species of PM$_{10}$ were used as input in the PCA. The KMO value was 0.81. A total of 5 principal components were extracted, with a total variance of 75.4% explained. Species with factor loading values > 0.4 were analyzed to identify sources. Figure 6 presents the principal components in terms of their factor loadings.

In PC1, EC, Al, Zn, Cl$^-$, K$^+$, and Fe showed substantial positive values with a variance of 37.0%. Dominant markers such as EC are vital tracers emitted from combustion sources and tracers of vehicular emissions (VEs) emitted globally [126,127]. Zn, Cl$^-$, and K$^+$ were

also traced in considerable amounts, and are attributed to the tailpipe emissions of two-stroke engines in which Zn is employed as a fuel additive, while K^+ is released from diesel exhausts [128–130]. PC1 was classified as VEs with a 9% contribution to PM_{10} concentration (Table S7). PC2 is considered a secondary aerosol (SA), as its precursors dominate (NO_3^-, SO_4^{2-}, and NH_4^+). SAs are produced from precursors such as NO_x, and SO_2, and NH_4^+ as $(NH_4)_2SO_4$ and NH_4NO_3 [131–133]. PC2 contributes 17% to the PM_{10} mass and explains the variance of 11.6%. PC3 is defined as a combined source of BB and fossil fuel combustion (FFC) as a combustion source. The precursors of BB (OC, EC, WSOC, and K^+) and FFC (Cl^-, F^-, OC, EC, S) showed strong and moderately positive factor loadings with a variance of 11%. This source majorly contributed to the PM_{10} mass concentration (35%), possibly due to enhanced burning activities at the study site and long-range transport from the IGP region (Figure 8). Globally, OC, EC, WSOC, K^+, Cl^-, F^-, OC, S, Mg^{2+}, and NH_4^+ are considered markers of combustion sources [4,131,133,134]. PC4 was classified as an SD as the crustal elements (Al, Zn, and Fe) showed strong positive loading values along with OC and EC, which are associated with SD emissions [45,135,136]. SD emissions showed the highest % contribution (38%), supported by the high concentration of crustal elements in trace and heavy elements over the study sites. PC5 showed substantial loadings of Mg^{2+}, Ca^{2+}, and Cl^-, tracers of sea salt (SS) aerosols (Na^+, Cl^-, Mg^{2+}, Ca^{2+}, and K^+) [87,137], with a total variance of 5.7%. As the study sites are far from any marine source, this factor was classified as sodium magnesium salts (SMS), contributing to 2% of the PM_{10} mass concentration (Figure 8).

Nainital

A total of 86 samples with 22 chemical species were used to identify the sources over Nainital. The KMO value was 0.83. A total of 5 principal components were extracted, with an explained variance of 80.6%. Chemical variables with factor loading values > 0.5 were chosen to identify sources. Figure 8 represents the principal components in terms of their factor loadings.

PC1 was defined as an SD as its high loading values were reflected by crustal components (Al, P, S, Ti, Fe, Mg, and Ca) [128,135–137]. This component explained a variance of 50.3% with a 25% contribution to PM_{10}, which is supported by earlier studies [71] and significant correlations of Al with Fe, Ca, Mg, and Ti (Figure S4). PC2 showed strong positive loadings of OC, EC, WSOC, K^+, and Mo, which are the markers for BB [4,110,131,133,137], delineating the source as BB with a variance of 11.1% and mass contribution of 20% to PM_{10}. PC3, defined as an SA, showed strong positive loadings of SO_4^{2-}, NO_3^-, and NH_4^+ with a variance of 7% and contributed to the mass concentration by 31%. PC4 inferred source VEs as tracers of VEs (EC, S, Zn, Na^+, and Zr), which have significant positive loadings with a 15% contribution to PM_{10}. PC5 represents SMS and contributed 9% to the PM_{10} mass. PC5 showed strong positive loading of Na^+, Mg, Br, and Cl^-; it could be identified as the long-range transport of aged sea spray and Cl^- depletion, as the influence of marine air masses is feeble at Nainital [71,76,91]. Sharma et al. [138] used the PCA model to identify crustal/SD, BB, and IE as the dominant sources of PM_{10} over the central Himalayas of India. Dumka et al. [139] revealed lesser contributions from the FFC and hydrophobic biofuels, whereas there was a higher contribution of hygroscopic pollutants for CCN formation from the IGP.

Darjeeling

A total of 135 samples with 22 chemical species were used in the analysis. The KMO value was 0.81. A total of 6 principal components were extracted, with an explained variance of 72.6%. Chemical variables with factor loading values > 0.5 were chosen to identify sources. Figure 7 represents the principal components in terms of their factor loadings.
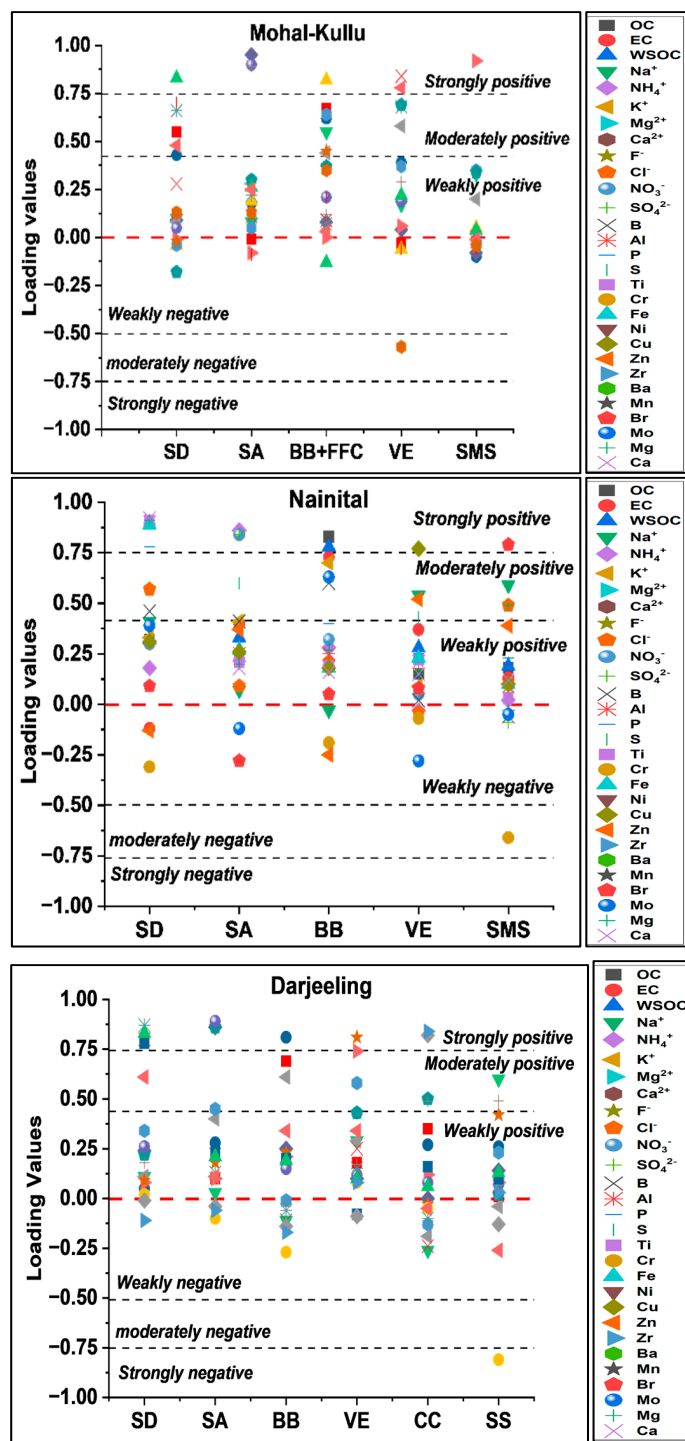
Figure 8. Source profiles obtained by PCA/APCS analyses of PM_{10} at the different study sites.

PC1 showed strong positive soil/crustal/road dust markers (Al, Ti, Fe, and Zn) loadings. PC1 explained a variance of 33.5% and the highest percentage contribution (31%) to the PM_{10} mass and was identified as an SD; it was also supported by transported soil re-suspension dust (Figure 8) and enrichment factors of elements as crustal or natural sources [72]. PC2 showed strong positive loadings of SAs (NO_3^-, SO_4^{2-}, and NH_4^+), with a variance of 12.5% and 21% contributions to the PM_{10} mass. PC3 was inferred as BB, and showed a variance of 9.1% and 28% contributions to the PM_{10} mass with significant loadings of markers associated with BB (OC, EC, WSOC, and K^+); significant contributions of carbonaceous components (OC, EC, and WSOC) and their relations also support BB as

a source of PM_{10} over Darjeeling. PC4 showed significant loadings of VEs (EC, F^-, Cl^-, Mg^{2+}, Ti, Ni, and Zn) markers with a 12% contribution to the PM_{10} mass as the study site experiences increased tourist activities, which might be contributing to PM from vehicle emissions. PC5 showed a variance of 5.9% and 5% contributions to the PM_{10} mass. PC5 was inferred as coal combustion, with significant SO_4^{2-}, Cl^-, OC, EC, Cu, and Zr loadings, as the Darjeeling site has local coal combustion (CC) emissions from the toy train of the Darjeeling Himalayan Railway: DHR [61,62,64]. PC6 showed a variance of 5.3% and only 3% contributions to the PM_{10} mass. PC5 showed significantly positive loadings of Na^+, Cl^-, and F^-, which are markers of SS aerosols. The site is influenced by transported air masses from marine sources (BoB), particularly in the monsoon season (Figure 6) [62,137]. According to previous studies [26,61,72], the common sources of particulate pollution identified using PCA are BB, SD, FFC, VEs, SS, and IE.

3.4.2. UNMIX
Mohal-Kullu

The high concentrations of Na^+, Mg^{2+}, Cl^-, and Ca^{2+} in source 1 were identified as an SMS, with a 4% contribution to the PM_{10} mass. Source 2 was inferred as a combustion source (BB+FFC) due to the presence of OC, EC, WSOC, Na^+, B, Al, NH_4^+, K^+, and Cl^- with a contribution of 45% to the PM_{10} mass concentration. Source 3 was designated as an SD due to high concentrations of Al, Fe, and Ca^{2+}, along with OC and EC, contributing 26% to the PM_{10} mass. The significant concentrations of NO_3^-, SO_4^{2-}, and NH_4^+ indicated source 4 as an SA with a 24% contribution to the PM_{10} mass (Figure 9).

Nainital

The high concentrations of OC, EC, and NO_3^- indicated source 1 as VEs, with a 7% contribution to the PM_{10} mass. Source 2 was identified as an SMS due to the presence of Na^+, Mg^{2+}, and Cl^-, with a contribution of 3% to the PM_{10} mass concentration. Source 3 was designated as dust (soil/mineral dust) due to high concentrations of Al, Fe, Zn, and Ca, along with OC and EC, contributing 37% to the PM_{10} mass. The significant presence of BB markers (OC, EC, WSOC, Fe, and SO_4^{2-}) indicated source 4 as BB and contributed 19% to the PM_{10} mass. Source 5 is inferred as an SA with a 34% contribution to PM_{10}, showing high loadings of NO_3^-, SO_4^{2-}, and NH_4^+ (Figure 9).

Darjeeling

The high concentrations of OC, EC, WSOC, Cl^-, and K^+ inferred source 1 as a CC, with a 7% contribution to the PM_{10} mass. Source 2 was identified by the occurrence of high concentrations of NO_3^-, SO_4^{2-}, and NH_4^+, marking source 2 as an SA and contributing 33% to the PM_{10} mass. Source 3 constituted high concentrations of OC, EC, WSOC, B, and NO_3^-, indicating this source as VEs, with a 7% contribution to the PM_{10} mass. Source 4 was designated as a BB source due to the presence of OC, EC, WSOC, Na^+, B, Al, NH_4^+, and K+, contributing 26% to the PM_{10} mass concentration. Source 5 was designated as SD/crustal dust due to high Al, Fe, Ca, OC, and EC concentrations, contributing 17% to the PM_{10} mass (Figure 9). Ghosh et al. [62] reported BB plumes from the IGP and local anthropogenic activities as the dominant source of coarse-mode aerosols.

3.4.3. PMF
Mohal-Kullu

The PMF model was run with 55 samples for 21 species in robust mode. At 5% extra modeling uncertainty, 95% of the Q values were near Q_{true} (1124), indicating a global minimum Q value. A four-factor solution was optimized based on PMF bootstrap (BS), displacement (DISP), and BS-DISP error, observed and modeled concentrations, and variability of the Q/Qexp ratio (<2). The Supplementary Materials provide a detailed model and error estimation summary (Table S2). The PMF model identified four sources (FFC, SAs, BB, and SD) (Figure 10).
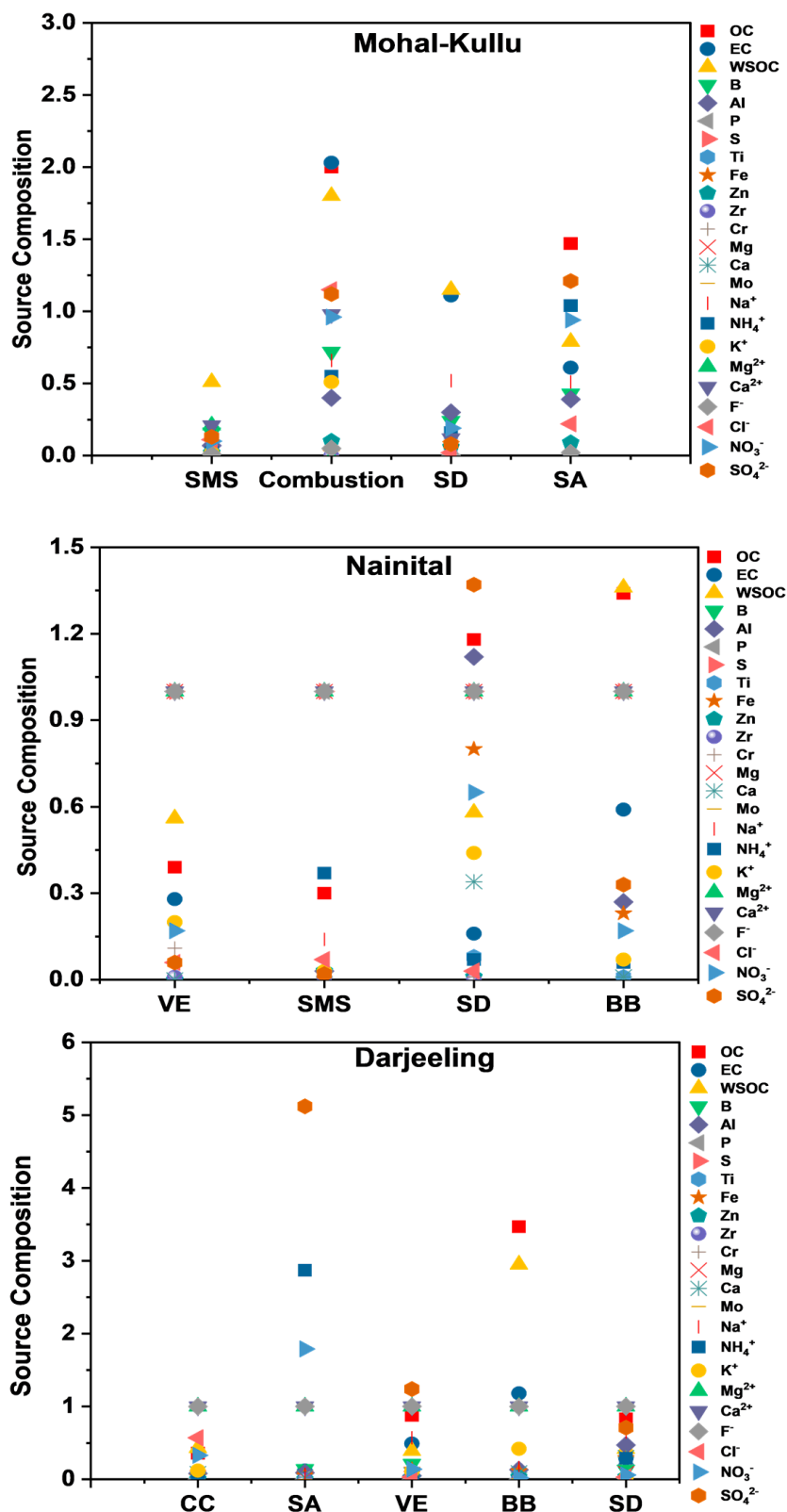
Figure 9. Source composition by UNMIX analysis for the identified PM$_{10}$ sources at the different study sites.
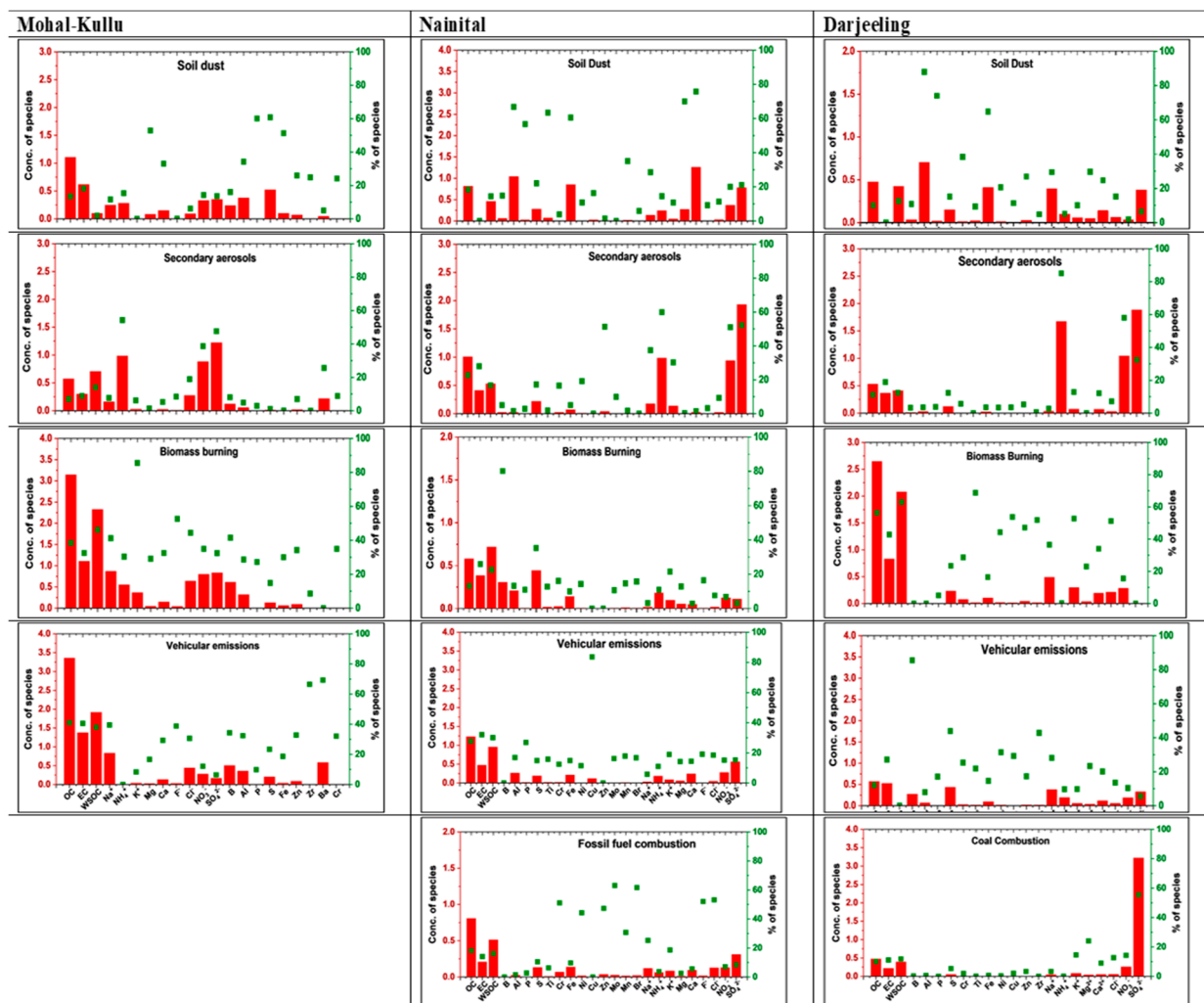
Figure 10. Percentage contribution of PM_{10} sources identified by PMF at the different study sites.

Source 1 is characterized by dominant species of OC, EC, F^-, Cl^-, Zn, Zr, Cr, and Al inferred as VEs. This source's abundance of EC, Al, Zn, and Cl^- indicates the intrusion from vehicular exhaust and non-exhaust emissions. The VEs source contributed approximately 29% to the PM_{10} mass at Mohal-Kullu. The mass ratio of $NO_3^-/SO_4^{2-} < 1$ also indicated the source of PM_{10} as being of anthropogenic origin [81]. Source 2 showed the dominant key markers of SAs (NO_3^-, SO_4^{2-}, and NH_4^+). SAs contributed 13% to the PM_{10} mass concentration and are derived from their gaseous precursors (SO_2 and NO_2) [61]. BB was defined as source 3 due to the predominant contribution of OC, EC, K^+, WSOC, NH_4^+, SO_4^{2-}, Cl^-, Zn, and Cr. Globally, K^+ is used as a marker of BB due to its release during the combustion process. The presence of carbonaceous species along with K^+ was attributed to BB, including vegetative/wood burning, agricultural residue, waste burning, and cow dung burning [110]. The presence of NH_4^+ along with K^+ and SO_4^{2-} confirmed the emissions were from BB [81]. The mass ratio of OC/EC > 2 also supported BB as a source of PM_{10} at the study site and contributed 34% to the PM_{10} mass concentration. Source 4 was characterized mainly by crustal elements (Mg, Ca, Al, P, Fe, and Zn) and contributed 23% to the PM_{10} mass. As explained, coarse-mode particles have significant contributions to crustal elements; this factor represents the SD source. Air mass backward trajectory also supports SD sources as long-range transport of particulates in the dry season carries dust-laden air masses from the Thar desert and the IGP region over the Himalayan region (Figure 7). Soni et al. [70] reported seasonal sources of PM_{10} using the PMF model, viz., soil/road dust (56%), VEs (32%), and IE (12%) in the summer season, whereas BB+VEs

(62%), IE (16%), soil/road dust (16%) and anthropogenic combustion (6%) were reported in the winter season. Kant et al. [140] identified probable sources of BC emanating from the northwest and eastern parts of the IGP, which are predominantly crop residue burning and forest fire zones in India.

Nainital

The PMF model was run with 86 samples for 25 species in robust mode. At 2% extra modeling uncertainty, 99% of the Q values were near Q_{true} (1303) for a 5-factor solution. The final solution was optimized based on BS, DISP, and BS-DISP errors, observed and modeled concentrations, and explained variability by the Q/Q_{exp} ratio. A detailed model summary and an error estimation summary are provided in the Supplementary Materials (Table S3). The PMF model identified five sources (SD, SAs, BB, FFC, and VEs) (Figure 10).

Source 1 is characterized by the higher contribution of Al, Mg, Ca, Ti, and Fe, corresponding to the factor as an SD, with a 26% contribution to the PM_{10} mass. Globally, several researchers have identified a wide range of elements (Al, Si, Ca, Ti, Fe, Cu, Mg, Mn, and Zn) as dust particles [45,126,134–136]. Air mass backward trajectories show that southwest monsoon air flows over the Arabian Sea, and dust-loaded air masses from the Thar desert and the IGP region arriving at the receptor site are also notable (Figure 7). Significant correlations of crustal elements also support SD as a primary source of PM_{10} at Nainital (Figure S4). High contributions of NO_3^-, SO_4^{2-}, and NH_4^+ inferred source 2 as an SA and contributed 18% to the PM_{10} mass concentration. Factor 3 is related to BB and was identified by the high contributions of BB markers (OC, EC, WSOC, K^+, and S). BB contributed 15% to the PM_{10} mass concentration. Generally, K^+ is used as a marker of BB, including cow dung, agricultural waste, crop residues, residential waste, vegetation, and wood [110]. The diagnostic ratios of nss K^+/EC, K^+/Cl^-, and K^+/NO_3^- supported BB as a source (Table S6 in the Supplementary Materials). During the summer season, crop residue burning is enhanced in northern India [66], and this region especially experiences forest fires, which might be a reason for BB as a source. Source 4 is characterized by dominant species of F^-, Cl^-, Br, Cr, Zn, Ni, OC, and EC, which were inferred as FFC. This source's abundance of F^- and Cl^- indicates the invasion of CC. The FFC source contributed approximately 22% to the PM_{10} mass at Nainital. Rabha et al. [132] also reported similar markers for CC in brick kilns and petroleum refineries in Jorhat, Northeast India. Source 5 showed notably high contributions of attributes such as OC, EC, and Cu, along with NO_3^-, Al, Cr, Mn, Cl^-, and Mo, which indicate VEs. VEs contributed 19% to the PM_{10} mass. Several researchers reported that OC, EC, NO_3^-, and Cl^- were profoundly emitted from tailpipe emissions of two-stroke engine and diesel exhausts [129,130,141–143]. Globally, Zn, Mn, Cu, and Al are non-exhaust markers from traffic sources such as clutch/tire, brake lining, and piston wear [131,139–142]. Zn and Mn were used as fuel additives [133,144–147] and significantly contributed to the VEs source. Our findings are supported by a recent study [71] which reported mineral dust (34%), BB (27%), secondary SO_4^{2-} (20%), secondary NO_3^- (9%), and mixed aerosols (10%) as the major sources of total suspended particulates (TSP) using the PMF model over the central Himalayas.

Darjeeling

The PMF model was run with 134 samples for 23 species in robust mode. At 2% extra modeling uncertainty, 99% of the Q values were near Q_{true} (2195), indicating a global Q value minimum for a 5-factor solution. The final solution was optimized based on the PMF BS, DISP, and BS-DISP errors, observed and modeled concentrations, and variability (Q/Q_{exp} ratio < 2). The Supplementary Materials provides a detailed model and error estimation summary (Table S4). The PMF model identified a total of five sources (SD, SAs, BB, CC, and VEs) (Figure 10).

The high contribution of SO_4^{2-}, Zn, Cl^-, and Cu in source 1 was inferred as CC. The higher contribution of SO_4^{2-} and Cl^- might be due to local CC-related emissions [44,134,137] from coal engines used in Darjeeling railways and transportation of advected burning

plumes from the IGP under favorable meteorological conditions. CC contributed 8% to the PM_{10} mass. Source 2 showed markers of SD re-suspension components (Al, P, Ti, Cr, Fe, Zn, Mo, Ca^{2+}, and Mg^{2+}) with a 23% contribution to the PM_{10} mass. Several researchers reported various elements as tracers of SD or crustal re-suspension [45,124,134–136]. Re-suspended dust from local and regional transport from the north and northwest of India significantly supports resuspended SD as a source of PM_{10} over Darjeeling (Figure 7). Source 3 showed the highest contribution of 32% to the PM_{10} mass with significant markers of BB (OC, EC, WSOC, K^+, Cu, Cr, Ni, Zn, Zr, and $Cl^−$). Globally, K^+ is a major marker of BB, resulting from the regional transport of BB plumes and local fire activities for domestic purposes [62]. Studies by researchers [14,61,62,144–148] supported the result that BB is a foremost source of PM at Darjeeling. Source 4 showed a significant contribution of markers for VEs (EC, Zr, B, Ti, Cr, Ni, and Cu), thus inferring the source as VEs. EC, $SO_4^{2−}$, $Cl^−$, and Zn are emitted from two-stroke engines and diesel exhausts. Zn and Ni are emitted from tire and brake wear [134]. VEs contributed 23% to the PM_{10} mass concentration over Darjeeling. Source 5 showed significant contributions from $NO_3^−$, $SO_4^{2−}$, and NH_4^+ with a 14% contribution to the PM_{10} mass. These markers are associated with the formation of secondary anthropogenic particles in the atmosphere. They are inferred as SAs due to Darjeeling having many tea gardens that use ammoniated fertilizers. Agricultural activities are the major sources of NH_4^+ in the atmosphere, supporting SAs as a source in Darjeeling. In 2014, Sarkar et al. [149] identified 8 sources of VOCs using the PMF model: gasoline exhaust (29%), diesel exhaust (32%), paint and solvent (18%), solid waste disposal (6%), household products (6%), IE (4%), CC (3%), and asphalt-related emissions (2%). Whereas in 2017, Sarkar et al. [150] reported that biogenic emissions (tea plants) and VEs are the major sources of carbonyl compounds over Darjeeling.

3.5. Model Comparison

The present study aimed to compare PM_{10} SA results for the IHR: Mohal-Kullu (Western Himalayas), Nainital (Central Himalayas), and Darjeeling (Eastern Himalayas), using three RMs (PCA/APCS, UNMIX, and PMF) (Table 2, Tables S8 and S9). We assessed the performance of receptor models in identifying and quantifying sources and the degree of concurrence between them. All three models showed similar source types, although source counts and contributions for the sampling sites changed significantly. Figure S6 illustrates the differences in the findings and comparative source profiles for the study sites (Supplementary Materials).

Table 2. Comparison of average source contributions (percentage) to the PM_{10} mass concentration among the PCA/APCS, UNMIX, and PMF models.

Identified Sources	Mohal-Kullu			Nainital			Darjeeling		
	PCA	UNMIX	PMF	PCA	UNMIX	PMF	PCA	UNMIX	PMF
Soil dust (SD)	38	26	23	25	37	26	31	17	23
Secondary aerosols (SAs)	17	24	13	31	34	18	21	33	14
Biomass burning (BB)	-	-	34	20	19	15	28	26	32
Fossil fuel combustion (FFC/CC)	-	-	-	-	-	22	5	7	8
Vehicular emissions (VEs)	9	-	29	15	7	19	12	17	23
Sea salts (SS)/sodium magnesium salts (SMS)	2	4	-	9	3	-	3	-	-
Combustion (BB+FFC)	35	45	-	-	-	-	-	-	-

The primary benefit of the PMF model is that it can treat non-negative solutions in a meaningful way, unlike PCA/APCS and UNMIX, which both include negative values in the source profiles and produce less efficient results when trying to identify the original sources [43,94,148]. While the PMF model requires a sizable dataset, it is robust enough to account for data gaps and sensitivity levels below the minimum detection threshold. In addition, the PMF model controls individual influences by giving each data point its

weight according to how confident it is in the measurement (USEPA, 2008). For resolving weighted factorization and permitting the independent handling of elements, experimental uncertainties are utilized [94]. This helps PMF in obtaining reliable outcomes.

On the other hand, PCA/APCS and UNMIX exclusively employ concentration measurements without uncertainty weighting (instead, using a somewhat coarse approach to down-weight outliers and point-by-point inaccurate estimates to down-weight missing data and anomalies, respectively). For all sites, the PMF model offers a precise percentage contribution of identified sources by effectively distributing marker species to corresponding sources and predicting individual sources. In contrast, PCA-APCS and UNMIX produce complexities in identifying sources by amalgamating precursors from two or more different (mixed-type sources). The identification and contribution of sources of PM assessed by various RMs may differ [4,43,44,88,151–154]. Considering these criteria, it is clear why PMF values are preferable over PCA/APCS and UNMIX estimations of particulate matter sources. A detailed summary of model comparisons is available in our previous publications [44,133].

Although many investigations have been conducted on the chemical composition of PM over the Himalayan region, each composition can change due to diverse sources, chemical transformations, and secondary atmospheric processes that occur in high-altitude mountains. Therefore, systematic data collection and comprehensive chemical characterization are required for reliable source apportionment as it impacts variations in source contribution and differs depending on the sources of pollution and meteorological conditions over that period. Due to the availability of a large dataset collected simultaneously in three IHR locations and its characteristics and chemical profiles, this investigation allowed us to distinguish between local, regional, and transboundary sources. The present study fulfills the substantial variations and limitations of previous source apportionment studies by incorporating extensive chemical speciation and quantitative receptor modeling over the same region of the IHR.

4. Conclusions

The present study investigated the variability of chemical compositions (carbonaceous components: (OC, EC, WSOC), WSIIS, trace, and heavy elements), formation, and processes of secondary inorganic components in different seasons and atmospheric environments (a high-altitude site at Mohal-Kullu in the western Himalayas, Nainital in the central Himalayas, and Darjeeling in the eastern Himalayas along with meteorological parameters). The study was conducted from August 2018–December 2019, and the major findings are as follows:

- The highest annual average mass concentration of PM_{10} was observed at Nainital (62 ± 39 µg m^{-3}), followed by Mohal Kullu (58 ± 32 µg m^{-3}), and Darjeeling (52 ± 18 µg m^{-3}), which are higher than the NAAQS.
- CAs are the major contributor to the PM_{10} concentration at the IHR, significantly contributing to climate change and affecting the Earth's radiation balance. Enhanced burning activities, regional transport of pollution plumes to high altitudes, and meteorological conditions affect the region's air quality.
- The average concentration of crustal components (Ca, Al, Fe, K, and Na) was considerably higher at all study sites, suggesting that the re-suspension of SD and crustal elements were significant at high altitudes of the Himalayas.
- Dominant secondary ions (NH_4^+, SO_4^{2-}, and NO_3^-) suggest that the study sites were strongly influenced by anthropogenic sources from regional and long-range transport. Sufficient NH_4^+ is available to neutralize SO_4^{2-} and NO_3^- as ammonium sulfate and ammonium nitrate.
- PCA/APCS, UNMIX, and PMF were used for SA of PM_{10} at the study sites. Overall, resuspended SD, secondary inorganic aerosols, VEs, and combustion-related emissions such as BB, CC, and FFC are the major sources of PM_{10} identified by different models at the study sites.

The outcomes of the present study will inform plans and policymakers toward managing air quality in the Himalayan region. In addition, this study supports a thorough analysis of the PM_{10} mass and sources contributing to pollution over the IHR in different seasons individually to plan strategies for reducing pollutants. This effort should eventually determine whether or not a stricter standard is required for the Himalayan region. The results will be used to evaluate emissions inventories and climate model outputs for the Himalayas.

Supplementary Materials: The following supporting information can be downloaded at: https://www.mdpi.com/article/10.3390/atmos14050880/s1. Table S1. S/N of species and MDL used for calculation of uncertainty at different study sites. Table S2. Model summary and the results of error estimates at Mohal-Kullu PMF. Table S3. Model summary and the results of error estimates in PMF at Nainital. Table S4. Model summary and the results of error estimates in PMF at Darjeeling. Table S5. Annual and seasonal average concentration of PM_{10} and its elemental composition at study sites of IHR. Table S6. Diagnostic mass ratios of carbonaceous and water soluble inorganic ionic components of PM_{10} at different study sites. Table S7. PCA factor loadings of PM_{10} at different locations of IHR. Table S8. Source composition of PM_{10} sources by UNMIX at different study sites. Table S9. Percent contribution of PM_{10} sources by PMF at different study sites. Figure S1. Seasonal variations in the concentration of PM_{10} at different study sites (in $\mu g\ m^{-3}$). Figure S2. Seasonal variations in the concentration of carbonaceous components (OC, EC, WSOC, POC, SOC) of PM_{10} at different study sites (in $\mu g\ m^{-3}$). Figure S3. Pie chart showing percentage contribution of analyzed species to PM_{10} at study sites in IHR. Figure S4. Scatter plots between crustal elements Al with Mg/Ca/Fe, and Ti of PM_{10} at different study sites. Figure S5. Seasonal CE/AE ratio for aerosol acidity at study sites. Figure S6. Scatter plots between OC/EC, WSOC/OC, SOC/OC of PM_{10} at different study sites.

References

1. Xu, Y.; Wu, X.; Kumar, R.; Barth, M.; Diao, C.; Gao, M.; Lin, L.; Jones, B.; Meehl, G.A. Substantial Increase in the Joint Occurrence and Human Exposure of Heatwave and High-PM Hazards Over South Asia in the Mid-21st Century. *AGU Adv.* **2020**, *1*, e2019AV000103. [CrossRef]
2. Yang, Y.; Zhou, R.; Yan, Y.; Yu, Y.; Liu, J.; Di, Y.; Du, Z.; Wu, D. Seasonal Variations and Size Distributions of Water-Soluble Ions of Atmospheric Particulate Matter at Shigatse, Tibetan Plateau. *Chemosphere* **2016**, *145*, 560–567. [CrossRef] [PubMed]
3. Adams, P.; Seinfeld, J.; Koch, D.; Mickley, L.; Jacob, D. General Circulation Assessment of Direct Radiative Forcing by the Sulphate-Nitrate-Ammonium-Water Inorganic Aerosol System. *J. Geophys. Res.* **2001**, *106*, 1097–1111. [CrossRef]
4. Cesari, D.; Benedetto, G.E.D.; Bonasoni, P.; Busetto, M.; Dinoi, A.; Merico, E.; Chirizzi, D.; Cristofanelli, P.; Donateo, A.; Grasso, F.M.; et al. Seasonal Variability of $PM_{2.5}$ and PM10 Composition and Sources in an Urban Background Site in Southern Italy. *Sci. Total Environ.* **2018**, *612*, 202–213. [CrossRef]
5. Mahapatra, P.S.; Sinha, P.R.; Boopathy, R.; Das, T.; Mohanty, S.; Sahu, S.C.; Gurjar, B.R. Seasonal Progression of Atmospheric Particulate Matter over an Urban Coastal Region in Peninsular India: Role of Local Meteorology and Long-Range Transport. *Atmos. Res.* **2018**, *199*, 145–158. [CrossRef]
6. Ramanathan, V.; Crutzen, P.J.; Kiehl, J.T.; Rosenfeld, D. Aerosols, Climate, and the Hydrological Cycle. *Science* **2001**, *294*, 2119–2124. [CrossRef]
7. Lohmann, U.; Feichter, J. Global Indirect Aerosol Effects: A Review. *Atmos. Chem. Phys.* **2005**, *5*, 715–737. [CrossRef]
8. Seinfeld, J.H.; Pandis, S.N. *Atmospheric Chemistry and Physics: From Air Pollution to Climate Change*; John Wiley & Sons: New York, NY, USA, 1998; Volume 51.
9. Smithson, P.A. IPCC, 2001: Climate Change 2001: The Scientific Basis. Contribution of Working Group 1 to the Third Assessment Report of the Intergovernmental Panel on Climate Change. *Int. J. Climatol.* **2002**, *22*, 1144. [CrossRef]
10. Banoo, R.; Sharma, S.K.; Gadi, R.; Gupta, S.; Mandal, T. Seasonal Variation of Carbonaceous Species of PM10 Over Urban Sites of National Capital Region of India. *Aerosol Sci. Eng.* **2020**, *4*, 111–123. [CrossRef]
11. Bond, T.C.; Doherty, S.J.; Fahey, D.W.; Forster, P.M.; Berntsen, T.; DeAngelo, B.J.; Flanner, M.G.; Ghan, S.; Kärcher, B.; Koch, D.; et al. Bounding the Role of Black Carbon in the Climate System: A Scientific Assessment. *J. Geophys. Res. Atmos.* **2013**, *118*, 5380–5552. [CrossRef]
12. Hansen, J.; Sato, M.; Ruedy, R.; Nazarenko, L.; Lacis, A.; Schmidt, G.A.; Russell, G.; Aleinov, I.; Bauer, M.; Bauer, S.; et al. Efficacy of Climate Forcings. *J. Geophys. Res. Atmos.* **2005**, *110*, D18104. [CrossRef]
13. Lim, H.-J.; Turpin, B.J. Origins of Primary and Secondary Organic Aerosol in Atlanta: Results of Time-Resolved Measurements during the Atlanta Supersite Experiment. *Environ. Sci. Technol.* **2002**, *36*, 4489–4496. [CrossRef] [PubMed]
14. Mukherjee, S.; Dutta, M.; Ghosh, A.; Chatterjee, A. A Year-Long Study on $PM_{2.5}$ and Its Carbonaceous Components over Eastern Himalaya in India: Contributions of Local and Transported Fossil Fuel and Biomass Burning during Premonsoon. *Environ. Res.* **2022**, *212*, 113546. [CrossRef] [PubMed]
15. Bhuyan, P.; Deka, P.; Prakash, A.; Balachandran, S.; Hoque, R. Chemical Characterization and Source Apportionment of Aerosol over Mid Brahmaputra Valley, India. *Environ. Pollut.* **2018**, *234*, 997–1010. [CrossRef] [PubMed]
16. Lighty, J.S.; Veranth, J.M.; Sarofim, A.F. Combustion Aerosols: Factors Governing Their Size and Composition and Implications to Human Health. *J. Air Waste Manag. Assoc.* **2000**, *50*, 1565–1618. [CrossRef] [PubMed]
17. Pope, C.A.; Ezzati, M.; Dockery, D.W. Fine-Particulate Air Pollution and Life Expectancy in the United States. *N. Engl. J. Med.* **2009**, *360*, 376–386. [CrossRef]
18. Singh, G.K.; Choudhary, V.; Gupta, T.; Paul, D. Investigation of Size Distribution and Mass Characteristics of Ambient Aerosols and Their Combustion Sources during Post-Monsoon in Northern India. *Atmos. Pollut. Res.* **2020**, *11*, 170–178. [CrossRef]
19. Deng, X.; Shi, C.; Wu, B.; Yang, Y.; Jin, Q.; Wang, H.; Zhu, S.; Yu, C. Characteristics of the Water-Soluble Components of Aerosol Particles in Hefei, China. *J. Environ. Sci.* **2016**, *42*, 32–40. [CrossRef]
20. Kang, J.; Cho, B.C.; Lee, C.-B. Atmospheric Transport of Water-Soluble Ions (NO_3^-, NH_4^+ and Nss-SO_4^{2-}) to the Southern East Sea (Sea of Japan). *Sci. Total Environ.* **2010**, *408*, 2369–2377. [CrossRef]
21. Pathak, R.K.; Wu, W.S.; Wang, T. Summertime $PM_{2.5}$ Ionic Species in Four Major Cities of China: Nitrate Formation in an Ammonia-Deficient Atmosphere. *Atmos. Chem. Phys.* **2009**, *9*, 1711–1722. [CrossRef]
22. Gaonkar, C.V.; Kumar, A.; Matta, V.M.; Kurian, S. Assessment of Crustal Element and Trace Metal Concentrations in Atmospheric Particulate Matter over a Coastal City in the Eastern Arabian Sea. *J. Air Waste Manag. Assoc.* **2020**, *70*, 78–92. [CrossRef] [PubMed]
23. Mohammed, G.; Karani, G.; Mitchell, D. Trace Elemental Composition in PM10 and $PM_{2.5}$ Collected in Cardiff, Wales. *Energy Procedia* **2017**, *111*, 540–547. [CrossRef]
24. Guo, F.; Tang, M.; Wang, X.; Yu, Z.; Wei, F.; Zhang, X.; Jin, M.; Wang, J.; Xu, D.; Chen, Z.; et al. Characteristics, Sources, and Health Risks of Trace Metals in $PM_{2.5}$. *Atmos. Environ.* **2022**, *289*, 119314. [CrossRef]
25. Hsu, C.-Y.; Chiang, H.-C.; Lin, S.-L.; Chen, M.-J.; Lin, T.-Y.; Chen, Y.-C. Elemental Characterization and Source Apportionment of PM10 and $PM_{2.5}$ in the Western Coastal Area of Central Taiwan. *Sci. Total Environ.* **2016**, *541*, 1139–1150. [CrossRef] [PubMed]
26. Sharma, S.K.; Mukherjee, S.; Choudhary, N.; Rai, A.; Ghosh, A.; Chatterjee, A.; Vijayan, N.; Mandal, T. Seasonal Variation and Sources of Carbonaceous Species and Elements in $PM_{2.5}$ and PM10 over the Eastern Himalaya. *Environ. Sci. Pollut. Res.* **2021**, *28*, 51642–51656. [CrossRef]

27. Zhang, J.; Li, R.; Zhang, X.; Bai, Y.; Cao, P.; Hua, P. Vehicular Contribution of PAHs in Size Dependent Road Dust: A Source Apportionment by PCA-MLR, PMF, and Unmix Receptor Models. *Sci. Total Environ.* **2019**, *649*, 1314–1322. [CrossRef]

28. Hu, X.; Zhang, Y.; Ding, Z.; Wang, T.; Lian, H.; Sun, Y.; Wu, J. Bioaccessibility and Health Risk of Arsenic and Heavy Metals (Cd, Co, Cr, Cu, Ni, Pb, Zn and Mn) in TSP and $PM_{2.5}$ in Nanjing, China. *Atmos. Environ.* **2012**, *57*, 146–152. [CrossRef]

29. Liu, X.; Ouyang, W.; Shu, Y.; Tian, Y.; Feng, Y.; Zhang, T.; Chen, W. Incorporating Bioaccessibility into Health Risk Assessment of Heavy Metals in Particulate Matter Originated from Different Sources of Atmospheric Pollution. *Environ. Pollut.* **2019**, *254*, 113113. [CrossRef]

30. Huang, Y.; Wang, L.; Zhang, S.; Zhang, M.; Wang, J.; Cheng, X.; Li, T.; He, M.; Ni, S. Source Apportionment and Health Risk Assessment of Air Pollution Particles in Eastern District of Chengdu. *Environ. Geochem. Health* **2020**, *42*, 2251–2263. [CrossRef]

31. Kelly, F.J.; Fussell, J.C. Air Pollution and Public Health: Emerging Hazards and Improved Understanding of Risk. *Environ. Geochem. Health* **2015**, *37*, 631–649. [CrossRef]

32. Wambebe, N.M.; Duan, X. Air Quality Levels and Health Risk Assessment of Particulate Matters in Abuja Municipal Area, Nigeria. *Atmosphere* **2020**, *11*, 817. [CrossRef]

33. Agarwal, R.; Awasthi, A.; Singh, N.; Mittal, S.K.; Gupta, P.K. Epidemiological Study on Healthy Subjects Affected by Agriculture Crop-Residue Burning Episodes and Its Relation with Their Pulmonary Function Tests. *Int. J. Environ. Health Res.* **2013**, *23*, 281–295. [CrossRef] [PubMed]

34. Chameides, W.L.; Yu, H.; Liu, S.C.; Bergin, M.; Zhou, X.; Mearns, L.; Wang, G.; Kiang, C.S.; Saylor, R.D.; Luo, C.; et al. Case Study of the Effects of Atmospheric Aerosols and Regional Haze on Agriculture: An Opportunity to Enhance Crop Yields in China through Emission Controls? *Proc. Natl. Acad. Sci. USA* **1999**, *96*, 13626–13633. [CrossRef]

35. Charlson, R.J.; Schwartz, S.E.; Hales, J.M.; Cess, R.D.; Coakley, J.A.; Hansen, J.E.; Hofmann, D.J. Climate Forcing by Anthropogenic Aerosols. *Science* **1992**, *255*, 423–430. [CrossRef] [PubMed]

36. Cohen, A.J.; Brauer, M.; Burnett, R.; Anderson, H.R.; Frostad, J.; Estep, K.; Balakrishnan, K.; Brunekreef, B.; Dandona, L.; Dandona, R.; et al. Estimates and 25-Year Trends of the Global Burden of Disease Attributable to Ambient Air Pollution: An Analysis of Data from the Global Burden of Diseases Study 2015. *Lancet* **2017**, *389*, 1907–1918. [CrossRef] [PubMed]

37. Joshi, H.; Naja, M.; Srivastava, P.; Gupta, T.; Gogoi, M.; Babu, S. Long-Term Trends in Black Carbon and Aerosol Optical Depth Over the Central Himalayas: Potential Causes and Implications. *Front. Earth Sci.* **2022**, *10*, 851444. [CrossRef]

38. Ramgolam, K.; Favez, O.; Cachier, H.; Gaudichet, A.; Marano, F.; Martinon, L.; Baeza-Squiban, A. Size-Partitioning of an Urban Aerosol to Identify Particle Determinants Involved in the Proinflammatory Response Induced in Airway Epithelial Cells. *Part. Fibre Toxicol.* **2009**, *6*, 10. [CrossRef]

39. Wang, X.; Wang, W.; Yang, L.; Gao, X.; Nie, W.; Yu, Y.; Xu, P.; Zhou, Y.; Wang, Z. The Secondary Formation of Inorganic Aerosols in the Droplet Mode through Heterogeneous Aqueous Reactions under Haze Conditions. *Atmos. Environ.* **2012**, *63*, 68–76. [CrossRef]

40. Saarikoski, S.; Mäkelä, T.; Hillamo, R.; Aalto, P.; Kerminen, V.-M.; Kulmala, M. Physicochemical Characterization and Mass Closure of Size-Segregated Atmospheric Aerosols in Hyytiälä, Finland. *Boreal Environ. Res.* **2005**, *10*, 385–400.

41. Ambade, B.; Sankar, T.K.; Sahu, L.K.; Dumka, U.C. Understanding Sources and Composition of Black Carbon and $PM_{2.5}$ in Urban Environments in East India. *Urban Sci.* **2022**, *6*, 60. [CrossRef]

42. Patel, A.; Rastogi, N. Chemical Composition and Oxidative Potential of Atmospheric PM_{10} over the Arabian Sea. *ACS Earth Space Chem.* **2020**, *4*, 112–121. [CrossRef]

43. Banerjee, T.; Murari, V.; Kumar, M.; Raju, M.P. Source Apportionment of Airborne Particulates through Receptor Modeling: Indian Scenario. *Atmos. Res.* **2015**, *164–165*, 167–187. [CrossRef]

44. Jain, S.; Sharma, S.K.; Choudhary, N.; Masiwal, R.; Saxena, M.; Sharma, A.; Mandal, T.K.; Gupta, A.; Gupta, N.C.; Sharma, C. Chemical Characteristics and Source Apportionment of $PM_{2.5}$ Using PCA/APCS, UNMIX, and PMF at an Urban Site of Delhi, India. *Environ. Sci. Pollut. Res.* **2017**, *24*, 14637–14656. [CrossRef] [PubMed]

45. Pant, P.; Harrison, R. Critical Review of Receptor Modelling for Particulate Matter: A Case Study of India. *Atmos. Environ.* **2012**, *49*, 1–12. [CrossRef]

46. Sharma, S.K.; Sharma, A.; Saxena, M.; Choudhary, N.; Masiwal, R.; Mandal, T.; Sharma, C. Chemical Characterization and Source Apportionment of Aerosol at an Urban Area of Central Delhi, India. *Atmos. Pollut. Res.* **2015**, *7*, 110–121. [CrossRef]

47. Gautam, R.; Hsu, N.; Lau, W.; Tsay, S.-C.; Kafatos, M. Enhanced Pre-Monsoon Warming over the Himalayan-Gangetic Region from 1979 to 2007. *Geophys. Res. Lett.* **2009**, *36*, L07704. [CrossRef]

48. Hindman, E.; Upadhyay, B. Air Pollution Transport in the Himalayas of Nepal and Tibet during the 1995–1996 Dry Season. *Atmos. Environ.* **2002**, *36*, 727–739. [CrossRef]

49. Carrico, C.; Bergin, M.; Shrestha, A.; Dibb, J.; Gomes, L.; Harris, J. The Importance of Carbon and Mineral Dust to Seasonal Aerosol Properties in the Nepal Himalaya. *Atmos. Environ.* **2003**, *37*, 2811–2824. [CrossRef]

50. Cong, Z.; Kang, S.; Kawamura, K.; Liu, B.; Wan, X.; Wang, Z.; Gao, S.; Fu, P. Carbonaceous Aerosols on the South Edge of the Tibetan Plateau: Concentrations, Seasonality and Sources. *Atmos. Chem. Phys.* **2015**, *15*, 1573–1584. [CrossRef]

51. Ming, J.; Zhang, D.; Kang, S.; Tian, W. Aerosol and Fresh Snow Chemistry in the East Rongbuk Glacier on the Northern Slope of Mt. Qomolangma (Everest). *J. Geophys. Res. Atmos.* **2007**, *112*, D008618. [CrossRef]

52. Tripathee, L.; Kang, S.; Rupakheti, D.; Zhang, Q.; Huang, J.; Sillanpää, M. Water-Soluble Ionic Composition of Aerosols at Urban Location in the Foothills of Himalaya, Pokhara Valley, Nepal. *Atmosphere* **2016**, *7*, 102. [CrossRef]

53. Xu, J.-S.; Xu, M.-X.; Snape, C.; He, J.; Behera, S.N.; Xu, H.-H.; Ji, D.-S.; Wang, C.-J.; Yu, H.; Xiao, H.; et al. Temporal and Spatial Variation in Major Ion Chemistry and Source Identification of Secondary Inorganic Aerosols in Northern Zhejiang Province, China. *Chemosphere* **2017**, *179*, 316–330. [CrossRef] [PubMed]

54. Zhao, Z.; Cao, J.; Shen, Z.; Xu, B.; Zhu, C.; Chen, L.-W.A.; Su, X.; Liu, S.; Han, Y.; Wang, G.; et al. Aerosol Particles at a High-Altitude Site on the Southeast Tibetan Plateau, China: Implications for Pollution Transport from South Asia. *J. Geophys. Res. Atmos.* **2013**, *118*, 11360–11375. [CrossRef]

55. Zhao, Z.; Wang, Q.; Li, L.; Han, Y.; Ye, Z.; Pongpiachan, S.; Zhang, Y.; Liu, S.; Tian, R.; Cao, J. Characteristics of PM$_{2.5}$ at a High-Altitude Remote Site in the Southeastern Margin of the Tibetan Plateau in Premonsoon Season. *Atmosphere* **2019**, *10*, 645. [CrossRef]

56. Agarwal, A.; Satsangi, A.; Lakhani, A.; Kumari, K. Seasonal and Spatial Variability of Secondary Inorganic Aerosols in PM$_{2.5}$ at Agra: Source Apportionment through Receptor Models. *Chemosphere* **2019**, *242*, 125132. [CrossRef] [PubMed]

57. Singh, N.; Banerjee, T.; Raju, M.P.; Deboudt, K.; Sorek-Hamer, M.; Singh, R.S.; Mall, R. Aerosol Chemistry, Transport, and Climatic Implications during Extreme Biomass Burning Emissions over the Indo-Gangetic Plain. *Atmos. Chem. Phys.* **2018**, *18*, 14197–14215. [CrossRef]

58. Banoo, R.; Sharma, S.K.; Rani, M.; Mandal, T.K. Source and Source Region of Carbonaceous Species and Trace Elements in PM$_{10}$ over Delhi, India. *Environ. Sci. Proc.* **2021**, *8*, 2. [CrossRef]

59. Rastogi, N.; Sarin, M.M. Chemistry of Aerosols over a Semi-Arid Region: Evidence for Acid Neutralization by Mineral Dust. *Geophys. Res. Lett.* **2006**, *33*, L23815. [CrossRef]

60. Safai, P.D.; Raju, M.P.; Rao, P.S.P.; Pandithurai, G. Characterization of Carbonaceous Aerosols over the Urban Tropical Location and a New Approach to Evaluate Their Climatic Importance. *Atmos. Environ.* **2014**, *92*, 493–500. [CrossRef]

61. Chatterjee, A.; Adak, A.; Singh, A.; Srivastava, M.; Ghosh, S.; Tiwari, S.; Devara, P.; Raha, S. Aerosol Chemistry over a High Altitude Station at Northeastern Himalayas, India. *PLoS ONE* **2010**, *5*, e11122. [CrossRef]

62. Ghosh, A.; Patel, A.; Rastogi, N.; Sharma, S.K.; Mandal, T.; Chatterjee, A. Size-Segregated Aerosols over a High Altitude Himalayan and a Tropical Urban Metropolis in Eastern India: Chemical Characterization, Light Absorption, Role of Meteorology and Long Range Transport. *Atmos. Environ.* **2021**, *254*, 118398. [CrossRef]

63. Kumar, A.; Attri, A. Biomass Combustion a Dominant Source of Carbonaceous Aerosols in the Ambient Environment of Western Himalayas. *Aerosol Air Qual. Res.* **2016**, *16*, 519–529. [CrossRef]

64. Rai, A.; Mukherjee, S.; Choudhary, N.; Ghosh, A.; Chatterjee, A.; Mandal, T.; Sharma, S.K.; Kotnala, R. Seasonal Transport Pathway and Sources of Carbonaceous Aerosols at an Urban Site of Eastern Himalaya. *Aerosol Sci. Eng.* **2021**, *5*, 318–343. [CrossRef]

65. Ram, K.; Sarin, M.M.; Rengarajan, R.; Sudheer, A.K. Carbonaceous and Secondary Inorganic Aerosols during Wintertime Fog and Haze over Urban Sites in the Indo-Gangetic Plain. *Aerosol Air Qual. Res.* **2013**, *12*, 359–370. [CrossRef]

66. Ram, K.; Sarin, M.M.; Hegde, P. Long-Term Record of Aerosol Optical Properties and Chemical Composition from a High-Altitude Site (Manora Peak) in Central Himalaya. *Atmos. Chem. Phys. Discuss.* **2010**, *10*, 7435–7467. [CrossRef]

67. Ram, K.; Sarin, M.M. Spatio-Temporal Variability in Atmospheric Abundances of EC, OC and WSOC over Northern India. *J. Aerosol Sci.* **2010**, *41*, 88–98. [CrossRef]

68. Roy, A.; Chatterjee, A.; Sarkar, C.; Das, S.K.; Ghosh, S.K.; Raha, S. A Study on Aerosol-Cloud Condensation Nuclei (CCN) Activation over Eastern Himalaya in India. *Atmos. Res.* **2017**, *189*, 69–81. [CrossRef]

69. Srivastava, A.; Ram, K.; Singh, S.; Kumar, S.; Tiwari, S. Aerosol Optical Properties and Radiative Effects over Manora Peak in the Himalayan Foothills: Seasonal Variability and Role of Transported Aerosols. *Sci. Total Environ.* **2015**, *502*, 287–295. [CrossRef]

70. Soni, A.; Kumar, U.; Prabhu, V.; Shridhar, V. Characterization, Source Apportionment and Carcinogenic Risk Assessment of Atmospheric Particulate Matter at Dehradun, Situated in the Foothills of Himalayas. *J. Atmos. Sol.-Terr. Phys.* **2020**, *199*, 105205. [CrossRef]

71. Sheoran, R.; Dumka, U.; Kaskaoutis, D.; Grivas, G.; Ram, K.; Prakash, J.; Hooda, R.; Tiwari, R.; Mihalopoulos, N. Chemical Composition and Source Apportionment of Total Suspended Particulate in the Central Himalayan Region. *Atmosphere* **2021**, *12*, 1228. [CrossRef]

72. Choudhary, N.; Srivastava, P.; Dutta, M.; Mukherjee, S.; Rai, A.; Kuniyal, J.C.; Lata, R.; Chatterjee, A.; Naja, M.; Vijayan, N.; et al. Seasonal Characteristics, Sources and Pollution Pathways of PM$_{10}$ at High Altitudes Himalayas of India. *Aerosol Air Qual. Res* **2022**, *22*, 220092. [CrossRef]

73. Kuniyal, J.C.; Thakur, A.; Thakur, H.; Sharma, S.; Pant, P.; Rawat, P.; Moorthy, K.K. Aerosol Optical Depths at Mohal-Kullu in the Northwestern Indian Himalayan High Altitude Station during ICARB. *J. Earth Syst. Sci.* **2009**, *118*, 41–48. [CrossRef]

74. Kumar, R.; Naja, M.; Satheesh, S.; Ojha, N.; Joshi, H.; Sarangi, T.; Pant, P.; Dumka, U.; Hegde, P. Influences of the Springtime Northern Indian Biomass Burning over the Central Himalayas. *J. Geophys. Res.* **2011**, *116*, D015509. [CrossRef]

75. Sarangi, T.; Naja, M.; Ojha, N.; Kumar, R.; Lal, S.; Sethuraman, V.; Kumar, A.; Sagar, R.; Chandola, H. First Simultaneous Measurements of Ozone, CO, and NO y at a High-Altitude Regional Representative Site in the Central Himalayas: Ozone, CO, and NO y over the himalayas. *J. Geophys. Res.* **2014**, *119*, 1592–1611. [CrossRef]

76. Srivastava, P.; Naja, M. Characteristics of Carbonaceous Aerosols Derived from Long-Term High-Resolution Measurements at a High-Altitude Site in the Central Himalayas: Radiative Forcing Estimates and Role of Meteorology and Biomass Burning. *Environ. Sci. Pollut. Res.* **2021**, *28*, 14654–14670. [CrossRef]

77. Chatterjee, A.; Mukherjee, S.; Dutta, M.; Ghosh, A.; Ghosh, S.K.; Roy, A. High Rise in Carbonaceous Aerosols under Very Low Anthropogenic Emissions over Eastern Himalaya, India: Impact of Lockdown for COVID-19 Outbreak. *Atmos. Environ.* **2021**, *244*, 117947. [CrossRef]

78. Sarkar, S.; Khillare, P.S. Profile of PAHs in the Inhalable Particulate Fraction: Source Apportionment and Associated Health Risks in a Tropical Megacity. *Environ. Monit. Assess.* **2013**, *185*, 1199–1213. [CrossRef]

79. Chow, J.; Watson, J.; Chen, L.-W.A.; Arnott, W.; Moosmuller, H.; Fung, K. Equivalence of Elemental Carbon by Thermal/Optical Reflectance and Transmittance with Different Temperature Protocols. *Environ. Sci. Technol.* **2004**, *38*, 4414–4422. [CrossRef]

80. Hegde, P.; Vyas, B.M.; Aswini, A.R.; Aryasree, S.; Nair, P.R. Carbonaceous and Water-Soluble Inorganic Aerosols over a Semi-Arid Location in North West India: Seasonal Variations and Source Characteristics. *J. Arid Environ.* **2020**, *172*, 104018. [CrossRef]

81. Hegde, P.; Kawamura, K.; Joshi, H.; Naja, M. Organic and Inorganic Components of Aerosols over the Central Himalayas: Winter and Summer Variations in Stable Carbon and Nitrogen Isotopic Composition. *Environ. Sci. Pollut. Res.* **2016**, *23*, 6102–6118. [CrossRef]

82. Jolliffe, I.T.; Cadima, J. Principal Component Analysis: A Review and Recent Developments. *Philos. Trans. R. Soc. A Math. Phys. Eng. Sci.* **2016**, *374*, 20150202. [CrossRef] [PubMed]

83. Hallin, M.; Paindaveine, D.; Verdebout, T. Efficient R-Estimation of Principal and Common Principal Components. *J. Am. Stat. Assoc.* **2014**, *109*, 1071–1083. [CrossRef]

84. Thurston, G.D.; Spengler, J.D. A Quantitative Assessment of Source Contributions to Inhalable Particulate Matter Pollution in Metropolitan Boston. *Atmos. Environ. 1967* **1985**, *19*, 9–25. [CrossRef]

85. Gewers, F.L.; Ferreira, G.R.; Arruda, H.F.D.; Silva, F.N.; Comin, C.H.; Amancio, D.R.; Costa, L.D.F. Principal Component Analysis: A Natural Approach to Data Exploration. *ACM Comput. Surv.* **2021**, *54*, 1–34. [CrossRef]

86. Kitao, A. Principal Component Analysis and Related Methods for Investigating the Dynamics of Biological Macromolecules. *J* **2022**, *5*, 298–317. [CrossRef]

87. Kothai, P.; Saradhi, I.V.; Prathibha, P.; Hopke, P.K.; Pandit, G.G.; Puranik, V.D. Source Apportionment of Coarse and Fine Particulate Matter at Navi Mumbai, India. *Aerosol Air Qual. Res.* **2008**, *8*, 423–436.

88. Song, Y.; Xie, S.; Zhang, Y.; Zeng, L.; Salmon, L.G.; Zheng, M. Source Apportionment of $PM_{2.5}$ in Beijing Using Principal Component Analysis/Absolute Principal Component Scores and UNMIX. *Sci. Total Environ.* **2006**, *372*, 278–286. [CrossRef]

89. Chen, Z.; Ding, Y.; Jiang, X.; Duan, H.; Ruan, X.; Li, Z.; Li, Y. Combination of UNMIX, PMF Model and Pb-Zn-Cu Isotopic Compositions for Quantitative Source Apportionment of Heavy Metals in Suburban Agricultural Soils. *Ecotoxicol. Environ. Saf.* **2022**, *234*, 113369. [CrossRef]

90. Henry, R. Multivariate Receptor Modeling by N-Dimensional Edge Detection. *Chemom. Intell. Lab. Syst.* **2003**, *65*, 179–189. [CrossRef]

91. Hopke, P.K. Review of Receptor Modeling Methods for Source Apportionment. *J. Air Waste Manag. Assoc.* **2016**, *66*, 237–259. [CrossRef]

92. Peter, A.E.; Shiva Nagendra, S.M.; Nambi, I.M. Comprehensive Analysis of Inhalable Toxic Particulate Emissions from an Old Municipal Solid Waste Dumpsite and Neighborhood Health Risks. *Atmos. Pollut. Res.* **2018**, *9*, 1021–1031. [CrossRef]

93. Brown, S.G.; Eberly, S.; Paatero, P.; Norris, G.A. Methods for Estimating Uncertainty in PMF Solutions: Examples with Ambient Air and Water Quality Data and Guidance on Reporting PMF Results. *Sci. Total Environ.* **2015**, *518–519*, 626–635. [CrossRef] [PubMed]

94. Paatero, P.; Tapper, U. Positive Matrix Factorization: A Non-Negative Factor Model with Optimal Utilization of Error Estimates of Data Values. *Environmetrics* **1994**, *5*, 111–126. [CrossRef]

95. Zhang, Y.; Cai, J.; Wang, S.; He, K.; Zheng, M. Review of Receptor-Based Source Apportionment Research of Fine Particulate Matter and Its Challenges in China. *Sci. Total Environ.* **2017**, *586*, 917–929. [CrossRef] [PubMed]

96. Amato, F.; Alastuey, A.; Karanasiou, A.; Lucarelli, F.; Nava, S.; Calzolai, G.; Severi, M.; Becagli, S.; Gianelle, V.L.; Colombi, C.; et al. AIRUSE-LIFE$+$: A Harmonized PM Speciation and Source Apportionment in Five Southern European Cities. *Atmos. Chem. Phys.* **2016**, *16*, 3289–3309. [CrossRef]

97. Behera, S.N.; Sharma, M. Spatial and Seasonal Variations of Atmospheric Particulate Carbon Fractions and Identification of Secondary Sources at Urban Sites in North India. *Environ. Sci. Pollut. Res.* **2015**, *22*, 13464–13476. [CrossRef] [PubMed]

98. Dumka, U.C.; Kaskaoutis, D.G.; Srivastava, M.K.; Devara, P.C.S. Scattering and Absorption Properties of Near-Surface Aerosol over Gangetic–Himalayan Region: The Role of Boundary-Layer Dynamics and Long-Range Transport. *Atmos. Chem. Phys.* **2015**, *15*, 1555–1572. [CrossRef]

99. Dumka, U.C.; Kosmopoulos, P.G.; Ningombam, S.S.; Masoom, A. Impact of Aerosol and Cloud on the Solar Energy Potential over the Central Gangetic Himalayan Region. *Remote Sens.* **2021**, *13*, 3248. [CrossRef]

100. Rastogi, N.; Singh, A.; Sarin, M.M.; Singh, D. Temporal Variability of Primary and Secondary Aerosols over Northern India: Impact of Biomass Burning Emissions. *Atmos. Environ.* **2016**, *125*, 396–403. [CrossRef]

101. Deshmukh, D.; Tsai, Y.I.; Deb, M.; Zarmpas, P. Characteristics and Sources of Water-Soluble Ionic Species Associated with PM_{10} Particles in the Ambient Air of Central India. *Bull. Environ. Contam. Toxicol.* **2012**, *89*, 1091–1097. [CrossRef]

102. Safai, P.D.; Budhavant, K.B.; Rao, P.S.P.; Ali, K.; Sinha, A. Source Characterization for Aerosol Constituents and Changing Roles of Calcium and Ammonium Aerosols in the Neutralization of Aerosol Acidity at a Semi-Urban Site in SW India. *Atmos. Res.* **2010**, *98*, 78–88. [CrossRef]

103. Yang, Y.; Yang, X.; He, M.; Christakos, G. Beyond Mere Pollution Source Identification: Determination of Land Covers Emitting Soil Heavy Metals by Combining PCA/APCS, GeoDetector and GIS Analysis. *CATENA* **2020**, *185*, 104297. [CrossRef]

104. Zhou, M.; Zheng, G.; Wang, H.; Qiao, L.; Zhu, S.; Huang, D.; An, J.; Lou, S.; Tao, S.; Wang, Q.; et al. Long-Term Trends and Drivers of Aerosol PH in Eastern China. *Atmos. Chem. Phys.* **2022**, *22*, 13833–13844. [CrossRef]

105. Sun, Y.; Zhuang, G.; Huang, K.; Li, J.; Wang, Q.; Wang, Y.; Lin, Y.; Fu, J.S.; Zhang, W.; Tang, A.; et al. Asian Dust over Northern China and Its Impact on the Downstream Aerosol Chemistry in 2004. *J. Geophys. Res. Atmos.* **2010**, *115*, D012757. [CrossRef]

106. Chelani, A.; Gajghate, D.; Chalapatirao, C.; Devotta, S. Particle Size Distribution in Ambient Air of Delhi and Its Statistical Analysis. *Bull. Environ. Contam. Toxicol.* **2010**, *85*, 22–27. [CrossRef]

107. Priyadharshini, B.; Verma, S.; Chatterjee, A.; Sharma, S.K.; Mandal, T.K. Chemical Characterization of Fine Atmospheric Particles of Water-Soluble Ions and Carbonaceous Species in a Tropical Urban Atmosphere over the Eastern Indo-Gangetic Plain. *Aerosol Air Qual. Res.* **2019**, *19*, 129–147. [CrossRef]

108. Rengarajan, R.; Sarin, M.M.; Sudheer, A.K. Carbonaceous and Inorganic Species in Atmospheric Aerosols during Wintertime over Urban and High-Altitude Sites in North India. *J. Geophys. Res. Atmos.* **2007**, *112*, D008150. [CrossRef]

109. Saraswati; Sharma, S.K.; Saxena, M.; Mandal, T.K. Characteristics of Gaseous and Particulate Ammonia and Their Role in the Formation of Secondary Inorganic Particulate Matter at Delhi, India. *Atmos. Res.* **2019**, *218*, 34–49. [CrossRef]

110. Ram, K.; Sarin, M.M. Day–Night Variability of EC, OC, WSOC and Inorganic Ions in Urban Environment of Indo-Gangetic Plain: Implications to Secondary Aerosol Formation. *Atmos. Environ.* **2011**, *45*, 460–468. [CrossRef]

111. Satsangi, A. Water Soluble Ionic Species in Atmospheric Aerosols: Concentrations and Sources at Agra in the Indo-Gangetic Plain (IGP). *Aerosol Air Qual. Res.* **2013**, *13*, 1877–1889. [CrossRef]

112. Tanner, R.L. An Ambient Experimental Study of Phase Equilibrium in the Atmospheric System: Aerosol H^+, NH_4^+, SO_4^{2-}, NO^{3-}-$NH_3(g)$, $HNO_3(g)$. *Atmos. Environ.* **1982**, *16*, 2935–2942. [CrossRef]

113. Heo, J.-B.; Hopke, P.K.; Yi, S.-M. Source Apportionment of $PM_{2.5}$ in Seoul, Korea. *Atmos. Chem. Phys.* **2009**, *9*, 4957–4971. [CrossRef]

114. Rastogi, N.; Sarin, M.M. Quantitative Chemical Composition and Characteristics of Aerosols over Western India: One-Year Record of Temporal Variability. *Atmos. Environ.* **2009**, *43*, 3481–3488. [CrossRef]

115. Ryou, H.G.; Heo, J.; Kim, S.-Y. Source Apportionment of PM_{10} and $PM_{2.5}$ Air Pollution, and Possible Impacts of Study Characteristics in South Korea. *Environ. Pollut.* **2018**, *240*, 963–972. [CrossRef] [PubMed]

116. Saffari, A.; Hasheminassab, S.; Shafer, M.M.; Schauer, J.J.; Chatila, T.A.; Sioutas, C. Nighttime Aqueous-Phase Secondary Organic Aerosols in Los Angeles and Its Implication for Fine Particulate Matter Composition and Oxidative Potential. *Atmos. Environ.* **2016**, *133*, 112–122. [CrossRef]

117. Taghvaee, S.; Sowlat, M.H.; Mousavi, A.; Hassanvand, M.S.; Yunesian, M.; Naddafi, K.; Sioutas, C. Source Apportionment of Ambient $PM_{2.5}$ in Two Locations in Central Tehran Using the Positive Matrix Factorization (PMF) Model. *Sci. Total Environ.* **2018**, *628–629*, 672–686. [CrossRef]

118. Duan, F.; Liu, X.; Yu, T.; Cachier, H. Identification and Estimate of Biomass Burning Contribution to the Urban Aerosol Organic Carbon Concentrations in Beijing. *Atmos. Environ.* **2004**, *38*, 1275–1282. [CrossRef]

119. Xu, J.; Wang, Z.; Yu, G.; Qin, X.; Ren, J.; Qin, D. Characteristics of Water Soluble Ionic Species in Fine Particles from a High Altitude Site on the Northern Boundary of Tibetan Plateau: Mixture of Mineral Dust and Anthropogenic Aerosol. *Atmos. Res.* **2014**, *143*, 43–56. [CrossRef]

120. Lelieveld, J.; Evans, J.S.; Fnais, M.; Giannadaki, D.; Pozzer, A. The Contribution of Outdoor Air Pollution Sources to Premature Mortality on a Global Scale. *Nature* **2015**, *525*, 367–371. [CrossRef]

121. Kumar, P.; Yadav, S. Seasonal Variations in Water Soluble Inorganic Ions, OC and EC in PM10 and PM>10 Aerosols over Delhi: Influence of Sources and Meteorological Factors. *Aerosol Air Qual. Res.* **2016**, *16*, 1165–1178. [CrossRef]

122. Rawat, P.; Sarkar, S.; Jia, S.; Khillare, P.S.; Sharma, B. Regional Sulfate Drives Long-Term Rise in AOD over Megacity Kolkata, India. *Atmos. Environ.* **2019**, *209*, 167–181. [CrossRef]

123. Rana, A.; Dey, S.; Rawat, P.; Mukherjee, A.; Mao, J.; Jia, S.; Khillare, P.; Yadav, A.; Sarkar, S. Optical Properties of Aerosol Brown Carbon (BrC) in the Eastern Indo-Gangetic Plain. *Sci. Total Environ.* **2020**, *716*, 137102. [CrossRef]

124. Arun, B.; Aswini, A.R.; Gogoi, M.; Hegde, P.; Kompalli, S.; Sharma, P.; Babu, S. Physico-Chemical and Optical Properties of Aerosols at a Background Site (~4 Km a.s.l.) in the Western Himalayas. *Atmos. Environ.* **2019**, *218*, 117017. [CrossRef]

125. Sarkar, C.; Roy, A.; Chatterjee, A.; Ghosh, S.; Raha, S. Factors Controlling the Long-Term (2009–2015) Trend of $PM_{2.5}$ and Black Carbon Aerosols at Eastern Himalaya, India. *Sci. Total Environ.* **2018**, *656*, 280–296. [CrossRef]

126. Chelani, A.B.; Gajghate, D.G.; Devotta, S. Source Apportionment of PM_{10} in Mumbai, India Using CMB Model. *Bull. Environ. Contam. Toxicol.* **2008**, *81*, 190–195. [CrossRef]

127. Chow, J.C.; Watson, J.G. Review of $PM_{2.5}$ and PM_{10} Apportionment for Fossil Fuel Combustion and Other Sources by the Chemical Mass Balance Receptor Model. *Energy Fuels* **2002**, *16*, 222–260. [CrossRef]

128. Begum, B.A.; Biswas, S.K.; Hopke, P.K. Key Issues in Controlling Air Pollutants in Dhaka, Bangladesh. *Atmos. Environ.* **2011**, *45*, 7705–7713. [CrossRef]
129. Mansha, M.; Ghauri, B.; Rahman, S.; Amman, A. Characterization and Source Apportionment of Ambient Air Particulate Matter (PM$_{2.5}$) in Karachi. *Sci. Total Environ.* **2012**, *425*, 176–183. [CrossRef]
130. Raja, S.; Biswas, K.F.; Husain, L.; Hopke, P.K. Source Apportionment of the Atmospheric Aerosol in Lahore, Pakistan. *Water Air Soil Pollut.* **2010**, *208*, 43–57. [CrossRef]
131. Khare, P.; Baruah, B. prasad. Elemental Characterization and Source Identification of PM$_{2.5}$ Using Multivariate Analysis at the Suburban Site of North-East India. *Atmos. Res.* **2010**, *98*, 148–162. [CrossRef]
132. Saggu, G.S.; Mittal, S.K. Source Apportionment of PM$_{10}$ by Positive Matrix Factorization Model at a Source Region of Biomass Burning. *J. Environ. Manag.* **2020**, *266*, 110545. [CrossRef] [PubMed]
133. Jain, S.; Sharma, S.K.; Vijayan, N.; Mandal, T. Seasonal Characteristics of Aerosols (PM$_{2.5}$ and PM$_{10}$) and Their Source Apportionment Using PMF: A Four Year Study over Delhi, India. *Environ. Pollut.* **2020**, *262*, 114337. [CrossRef] [PubMed]
134. Rabha, S.; Islam, N.; Saikia, B.K.; Singh, G.K.; Qadri, A.M.; Srivastava, V.; Gupta, T. Year-Long Evaluation of Aerosol Chemistry and Meteorological Implications of PM$_{2.5}$ in an Urban Area of the Brahmaputra Valley, India. *Environ. Sci. Atmos.* **2023**, *3*, 196–206. [CrossRef]
135. Begum, B.A.; Biswas, S.K.; Markwitz, A.; Hopke, P.K. Identification of Sources of Fine and Coarse Particulate Matter in Dhaka, Bangladesh. *Aerosol Air Qual. Res.* **2010**, *10*, 345–353. [CrossRef]
136. Shridhar, V.; Khillare, P.S.; Agarwal, T.; Ray, S. Metallic Species in Ambient Particulate Matter at Rural and Urban Location of Delhi. *J. Hazard. Mater.* **2010**, *175*, 600–607. [CrossRef]
137. Kumar, A.; Suresh, K.; Rahaman, W. Geochemical Characterization of Modern Aeolian Dust over the Northeastern Arabian Sea: Implication for Dust Transport in the Arabian Sea. *Sci. Total Environ.* **2020**, *729*, 138576. [CrossRef]
138. Sharma, S.K.; Choudhary, N.; Srivastava, P.; Naja, M.; Vijayan, N.; Kotnala, G.; Mandal, T. Variation of Carbonaceous Species and Trace Elements in PM$_{10}$ at a Mountain Site in the Central Himalayan Region of India. *J. Atmos. Chem.* **2020**, *77*, 49–62. [CrossRef]
139. Dumka, U.; Kaskaoutis, D.; Mihalopoulos, N.; Sheoran, R. Identification of Key Aerosol Types and Mixing States in the Central Indian Himalayas during the GVAX Campaign: The Role of Particle Size in Aerosol Classification. *Sci. Total Environ.* **2020**, *761*, 143188. [CrossRef]
140. Kant, Y.; Darga Saheb, S.; Mitra, D.; Chandola, H.; Babu, S.; Chauhan, P. Black Carbon Aerosol Quantification over North-West Himalayas: Seasonal Heterogeneity, Source Apportionment and Radiative Forcing. *Environ. Pollut.* **2019**, *257*, 113446. [CrossRef]
141. Pant, P.; Harrison, R.M. Estimation of the Contribution of Road Traffic Emissions to Particulate Matter Concentrations from Field Measurements: A Review. *Atmos. Environ.* **2013**, *77*, 78–97. [CrossRef]
142. Roy, A.; Chatterjee, A.; Tiwari, S.; Sarkar, C.; Das, S.K.; Ghosh, S.K.; Raha, S. Precipitation Chemistry over Urban, Rural and High Altitude Himalayan Stations in Eastern India. *Atmos. Res.* **2016**, *181*, 44–53. [CrossRef]
143. Lodhi, A.; Ghauri, B.M.; Khan, M.; Rahmana, S.; Shafique, S. Particulate Matter (PM$_{2.5}$) Concentration and Source Apportionment in Lahore. *J. Braz. Chem. Soc. JBCS* **2009**, *20*, 1811–1820. [CrossRef]
144. Rai, P.; Furger, M.; El Haddad, I.; Kumar, V.; Wang, L.; Singh, A.; Dixit, K.; Bhattu, D.; Petit, J.-E.; Ganguly, D.; et al. Real-Time Measurement and Source Apportionment of Elements in Delhi's Atmosphere. *Sci. Total Environ.* **2020**, *742*, 140332. [CrossRef] [PubMed]
145. Song, S.; Wu, Y.; Jiang, J.; Yang, L.; Cheng, Y.; Hao, J. Chemical Characteristics of Size-Resolved PM$_{2.5}$ at a Roadside Environment in Beijing, China. *Environ. Pollut.* **2012**, *161*, 215–221. [CrossRef]
146. Srimuruganandam, B.; Shiva Nagendra, S.M. Chemical Characterization of PM$_{10}$ and PM$_{2.5}$ Mass Concentrations Emitted by Heterogeneous Traffic. *Sci. Total Environ.* **2011**, *409*, 3144–3157. [CrossRef]
147. Thorpe, A.; Harrison, R.M. Sources and Properties of Non-Exhaust Particulate Matter from Road Traffic: A Review. *Sci. Total Environ.* **2008**, *400*, 270–282. [CrossRef]
148. Yadav, S.; Tripathi, S.N.; Rupakheti, M. Current Status of Source Apportionment of Ambient Aerosols in India. *Atmos. Environ.* **2022**, *274*, 118987. [CrossRef]
149. Sarkar, C.; Chatterjee, A.; Majumdar, D.; Ghosh, S.; Srivastava, A.; Raha, S. Volatile Organic Compounds over Eastern Himalaya, India: Temporal Variation and Source Characterization Using Positive Matrix Factorization. *Atmos. Chem. Phys. Discuss.* **2014**, *14*, 32133–32175. [CrossRef]
150. Sarkar, C.; Chatterjee, A.; Majumdar, D.; Roy, A.; Srivastava, A.; Ghosh, S.; Raha, S. How the Atmosphere over Eastern Himalaya, India Is Polluted with Carbonyl Compounds? Temporal Variability and Identification of Sources. *Aerosol Air Qual. Res.* **2017**, *17*, 2206–2223. [CrossRef]
151. Amato, F.; Pandolfi, M.; Escrig, A.; Querol, X.; Alastuey, A.; Pey, J.; Perez, N.; Hopke, P.K. Quantifying Road Dust Resuspension in Urban Environment by Multilinear Engine: A Comparison with PMF2. *Atmos. Environ.* **2009**, *43*, 2770–2780. [CrossRef]
152. Contini, D.; Belosi, F.; Gambaro, A.; Cesari, D.; Stortini, A.M.; Bove, M.C. Comparison of PM$_{10}$ Concentrations and Metal Content in Three Different Sites of the Venice Lagoon: An Analysis of Possible Aerosol Sources. *J. Environ. Sci.* **2012**, *24*, 1954–1965. [CrossRef] [PubMed]

153. Favez, O.; El Haddad, I.; Piot, C.; Boréave, A.; Abidi, E.; Marchand, N.; Jaffrezo, J.-L.; Besombes, J.-L.; Personnaz, M.-B.; Sciare, J.; et al. Inter-Comparison of Source Apportionment Models for the Estimation of Wood Burning Aerosols during Wintertime in an Alpine City (Grenoble, France). *Atmos. Chem. Phys.* **2010**, *10*, 5295–5314. [CrossRef]
154. Sharma, S.K.; Mandal, T.K. Elemental composition and sources of fine particulate matter ($PM_{2.5}$) in Delhi, India. *Bull. Environ. Contamin. Toxicol.* **2023**, *110*, 60. [CrossRef] [PubMed]